



AMERICAN METEOROLOGICAL SOCIETY

Monthly Weather Review

EARLY ONLINE RELEASE

This is a preliminary PDF of the author-produced manuscript that has been peer-reviewed and accepted for publication. Since it is being posted so soon after acceptance, it has not yet been copyedited, formatted, or processed by AMS Publications. This preliminary version of the manuscript may be downloaded, distributed, and cited, but please be aware that there will be visual differences and possibly some content differences between this version and the final published version.

The DOI for this manuscript is doi: 10.1175/2008MWR2709.1

The final published version of this manuscript will replace the preliminary version at the above DOI once it is available.



**The maximum intensity of tropical cyclones in axisymmetric
numerical model simulations**

George H. Bryan and Richard Rotunno

National Center for Atmospheric Research,¹ Boulder, Colorado

Submitted to *Monthly Weather Review*

First submitted: 30 June 2008

Last modified: 26 November 2008

Corresponding author address: George H. Bryan, National Center for Atmospheric Research,
3450 Mitchell Lane, Boulder, CO 80301. E-mail: gbryan@ucar.edu

¹The National Center for Atmospheric Research is sponsored by the National Science Foundation.

Abstract

An axisymmetric numerical model is used to evaluate the maximum possible intensity of tropical cyclones. As compared to traditionally formulated nonhydrostatic models, this new model has improved mass and energy conservation in saturated conditions. Compared to the axisymmetric model developed by Rotunno and Emanuel, the new model produces weaker cyclones (by $\sim 10\%$, in terms of maximum azimuthal velocity); the difference is attributable to several approximations in the Rotunno-Emanuel model. Then, using a single specification for initial conditions (with sea surface temperature of 26°C), the authors conduct model sensitivity tests to determine the sensitivity of maximum azimuthal velocity (v_{\max}) to uncertain aspects of the modeling system. For fixed mixing lengths in the turbulence parameterization, a converged value of v_{\max} is achieved for radial grid spacing of order 1 km and vertical grid spacing of order 250 m. The fall velocity of condensate (V_t) changes v_{\max} by up to 60%, and the largest v_{\max} occurs for pseudoadiabatic thermodynamics (that is, for $V_t > 10 \text{ m s}^{-1}$). The sensitivity of v_{\max} to the ratio of surface exchange coefficients for entropy and momentum (C_E/C_D) matches the theoretical result, $v_{\max} \sim (C_E/C_D)^{1/2}$, for nearly inviscid flow, but simulations with increasing turbulence intensity show less dependence on C_E/C_D ; this result suggests that the effect of C_E/C_D is less important than has been argued previously. The authors find that v_{\max} is most sensitive to the intensity of turbulence in the radial direction. However, some settings, such as inviscid flow, yield clearly unnatural structures; for example, v_{\max} exceeds 110 m s^{-1} , despite a maximum observed intensity of $\sim 70 \text{ m s}^{-1}$ for this environment. The authors show that turbulence in the radial direction limits maximum axisymmetric intensity by weakening the radial gradients of angular momentum (which prevents environmental air from being drawn to small radius) and of entropy (which is consistent with weaker intensity by consideration of thermal wind balance). It is also argued that future studies should consider parameterized turbulence as an important factor in simulated tropical cyclone intensity.

1 Introduction

The theoretical maximum intensity of tropical cyclones has been a subject of much study recently. There are several possible applications for this subject, such as for real-time forecasting, for hazard planning and management, and for studying the consequences of climate change. Hence, a reasonable estimate for maximum intensity has clear value.

Several different strategies are used to explore this topic. We classify these approaches into three general categories. One is the analytic approach, which relies primarily upon the governing equations for the atmosphere and several assumptions about the processes that occur in tropical cyclones. This method has probably received the greatest attention, at least in the published literature. Notable techniques have been put forth recently by Emanuel (1986, 1988, 1995) and Holland (1997). These techniques are commonly referred to as potential intensity (PI) theories.

A second method is to use an entirely observational dataset. In this approach, statistical analysis is used to determine the maximum intensity as a function of observed environmental conditions (such as sea surface temperature). This approach was undertaken, for example, by DeMaria and Kaplan (1994), Whitney and Hobgood (1997), and Zeng et al. (2007).

A third method is to use a time-dependent numerical model. In this approach, a weak tropical cyclone is placed into a specified environment; the model is then integrated forward in time, the tropical cyclone intensifies, and ultimately a maximum intensity is achieved. This approach was undertaken, for example, using an axisymmetric numerical model by Rotunno and Emanuel (1987) and Persing and Montgomery (2005).

Of these three approaches, numerical modeling is probably the easiest to undertake, in the sense that little input is required of the model user. For example, as opposed to the analytic approach, numerical modeling does not require a great deal of knowledge about the flow to be studied; rather, given suitable initial and boundary conditions, then the numerical model will generate the flow of interest. Furthermore, as opposed to the observational approach, numerical modeling does not require a large dataset of observations; rather, the maximum

intensity can be studied in idealized environments, where only an environmental sounding, a sea-surface temperature, and a weak initial vortex need to be specified.

On the other hand, numerical modeling has several potential drawbacks. The governing equations and parameterizations need to accurately describe all important processes that occur in tropical cyclones. The grid spacing must be sufficiently small to resolve the important features of a tropical cyclone, and the effects of unresolved turbulent motions must be included accurately. Additionally, the model's numerical techniques must be sufficiently accurate so they do not affect the solution.

In this article, the maximum intensity of tropical cyclones is investigated using a time-dependent, axisymmetric, nonhydrostatic numerical model. The primary goal is to determine the maximum possible intensity of a tropical cyclone in the numerical model given a single specified set of initial conditions. Additionally, the sensitivity of model-produced maximum intensity is investigated by making changes to components of the model that have uncertain settings: examples include the grid spacing, the turbulence parameterization, the air-sea exchange coefficients, settings in the microphysics parameterization, and the governing equations of the model. The model-produced intensity is compared to the maximum value that has been observed for this environment, which helps identify processes that might be important for determining the maximum intensity of natural tropical cyclones. These results should be useful to numerical model developers, and they can also help guide the development of analytic PI theories.

An axisymmetric model is used herein because its small computational overhead allows us to investigate a large number of modeling components systematically. The primary drawback to axisymmetric models, of course, is the lack of three-dimensional features such as mesovortices in the eye/eyewall, boundary-layer roll vortices, upper-level asymmetric outflow jets, vortex Rossby waves, etc, which must be viewed as turbulence and accounted for by a parameterization. Hence, some results reported herein might be specific to axisymmetric models, and should someday be re-evaluated using three-dimensional numerical simulations.

2 Description of the numerical model

A new axisymmetric numerical model was developed for this study, to take advantage of recent advances in numerical model design. The model is based on the compressible nonhydrostatic cloud model of Bryan and Fritsch (2002). It is configured for axisymmetric simulations of tropical cyclones following the study by Rotunno and Emanuel (1987, hereafter referred to as RE87). Compared to the RE87 Model, there are several notable improvements in the new model, including: an equation set that mathematically conserves total mass and energy in reversible saturated conditions; the ability to include dissipative heating, which has been shown to increase hurricane intensity by as much as 20% (e.g., Bister and Emanuel 1998); and more accurate numerical techniques for split-explicit compressible models (e.g., Wicker and Skamarock 2002). There are, however, several similarities between these two models, including: both are compressible nonhydrostatic models; both use the same grid staggering; both use the same general approach for parameterization of turbulence; and, for all simulations in this article, both use the same simple methods to specify radiative and microphysical processes. Further details of the differences are provided below. Readers that are not interested in model details can skip ahead to section 3, which presents the primary results of this study.

a. Governing equations

The model equations are written in cylindrical coordinates (r, ϕ, z) , although, by assumption, no variation in ϕ is permitted herein. There are seven time-dependent variables: velocities in the radial, azimuthal, and vertical directions (u, v, w) ; perturbation nondimensional pressure, π' ; potential temperature, θ ; mixing ratio of water vapor, q_v ; and mixing ratio of liquid water, q_l . The governing equations for these variables are as follows:

$$\frac{\partial u}{\partial t} = -u \frac{\partial u}{\partial r} - w \frac{\partial u}{\partial z} + \left(f + \frac{v}{r}\right) v - c_p \theta_v \frac{\partial \pi'}{\partial r} + D_u + N_u, \quad (1)$$

$$\frac{\partial \bar{v}}{\partial t} = -u \frac{\partial \bar{v}}{\partial r} - w \frac{\partial \bar{v}}{\partial z} - \left(f + \frac{v}{r}\right) u + D_v + N_v, \quad (2)$$

$$\frac{\partial \bar{w}}{\partial t} = -u \frac{\partial \bar{w}}{\partial r} - w \frac{\partial \bar{w}}{\partial z} - c_p \theta_v \frac{\partial \pi'}{\partial z} + g \left(\frac{\theta'_v}{\bar{\theta}_v}\right) + D_w + N_w, \quad (3)$$

$$\frac{\partial \pi'}{\partial t} = -u \frac{\partial \pi}{\partial r} - w \frac{\partial \pi}{\partial z} - \Pi_1 \pi \left(\frac{1}{r} \frac{\partial r u}{\partial r} + \frac{\partial w}{\partial z}\right) + \Pi_2 \dot{q}_{\text{cond}} + \Pi_3 (\epsilon + D_\theta + N_\theta + R), \quad (4)$$

$$\frac{\partial \theta}{\partial t} = -u \frac{\partial \theta}{\partial r} - w \frac{\partial \theta}{\partial z} - \Theta_1 \theta \left(\frac{1}{r} \frac{\partial r u}{\partial r} + \frac{\partial w}{\partial z}\right) + \Theta_2 \dot{q}_{\text{cond}} + \Theta_3 \epsilon + D_\theta + N_\theta + R, \quad (5)$$

$$\frac{\partial q_v}{\partial t} = -u \frac{\partial q_v}{\partial r} - w \frac{\partial q_v}{\partial z} + D_{q_v} - \dot{q}_{\text{cond}}, \quad (6)$$

$$\frac{\partial q_l}{\partial t} = -u \frac{\partial q_l}{\partial r} - w \frac{\partial q_l}{\partial z} + D_{q_l} + \dot{q}_{\text{cond}} + \frac{1}{\rho_d} \frac{\partial (\rho_d q_l V_t)}{\partial z}. \quad (7)$$

Overbars refer to a one-dimensional (vertical) reference profile that is in hydrostatic balance [$d\bar{\pi}/dz = -g/(c_p \bar{\theta}_v)$], and primes refer to perturbations from this reference state. The definitions for π and θ are customary: $\pi \equiv (p/p_0)^{R_d/c_p}$ and $\theta \equiv T/\pi$, wherein p_0 is a reference pressure, c_p is the specific heat of dry air at constant pressure, R_d is the gas constant for dry air, and T is absolute temperature. Virtual potential temperature includes the effects of liquid water: $\theta_v \equiv \theta (1 + q_v R_v/R_d) / (1 + q_v + q_l)$, wherein R_v is the gas constant for water vapor. Other symbols are defined as follows: f is the Coriolis parameter; g is gravitational acceleration; the D symbols represent tendencies from turbulent motions (described below); N represents upper-level Newtonian damping used to eliminate vertically propagating gravity waves, following RE87 (p. 546); R is the term from RE87 (p. 546) that mimics radiative cooling throughout the domain; \dot{q}_{cond} is the rate of condensation/evaporation between vapor and liquid; ρ_d is density of dry air, determined using the ideal gas law, $\rho_d = p_0 \pi^{c_v/R_d} (R_d \theta (1 + q_v R_v/R_d))^{-1}$; and V_t is the terminal fall velocity of liquid water. The symbols Θ_3 and ϵ are associated with dissipative heating and are explained below.

The remaining undefined symbols — Π_1 , Π_2 , Π_3 , Θ_1 , and Θ_2 — are associated with the conservation of mass and internal energy in moist flows. These variables can be formulated in two ways. One yields an approximate equation set that is traditionally used for

nonhydrostatic cloud models, and is very similar to the equations used by RE87:

$$\Pi_1 = \frac{R_d}{c_v}, \quad \Pi_2 = 0, \quad \Pi_3 = 0, \quad (8)$$

$$\Theta_1 = 0, \quad \Theta_2 = \frac{L_v}{c_p \pi}, \quad (9)$$

wherein L_v is the latent heat of vaporization and c_v is the specific heat of dry air at constant volume. With this formulation, hereinafter referred to as the “traditional equation set,” the model cannot conserve mass and internal energy. The second formulation, derived by Bryan and Fritsch (2002) and hereinafter referred to as the “conservative equation set,” allows the total mass and internal energy to be conserved in a reversible moist environment, and the appropriate formulations are

$$\Pi_1 = \frac{R_d c_{pm}}{c_p c_{vm}}, \quad \Pi_2 = \frac{R_d}{c_p} \left(\frac{L_v}{c_{vm} \theta} - \pi \frac{R_v c_{pm}}{R_m c_{vm}} \right), \quad \Pi_3 = \frac{R}{c_v} \frac{\pi}{\theta}, \quad (10)$$

$$\Theta_1 = \left(\frac{R_m}{c_{vm}} - \frac{R_d c_{pm}}{c_p c_{vm}} \right), \quad \Theta_2 = \frac{c_v L_v}{c_{vm} c_p \pi} - \theta \frac{R_v}{c_{vm}} \left(1 - \frac{R_d c_{pm}}{c_p R_m} \right), \quad (11)$$

wherein variables for the mixture of moist, saturated air are defined as follows:

$$c_{pm} \equiv c_p + c_{pv} q_v + c_l q_l, \quad c_{vm} \equiv c_v + c_{vv} q_v + c_l q_l, \quad R_m \equiv R_d + R_v q_v, \quad (12)$$

and wherein c_{pv} and c_{vv} are the specific heats of water vapor at constant pressure and volume, respectively, and c_l is the specific heat of liquid water. Using these variables, a governing equation for total mass can be derived by using the ideal gas law, the definitions of mixing ratios, and using (4) – (7); for the conservative equation set, this yields

$$\frac{\partial \rho_t}{\partial t} + \frac{1}{r} \frac{\partial (r \rho_t u)}{\partial r} + \frac{\partial (\rho_t w)}{\partial z} = \frac{\partial (\rho_l V_l)}{\partial z} + D_{qt}, \quad (13)$$

wherein $\rho_t \equiv \rho_d + \rho_v + \rho_l$ is total density [the sum of the densities of dry air (ρ_d), water vapor (ρ_v), and liquid water (ρ_l)] and D_{qt} represents the tendency from turbulence (which,

we note, includes the surface flux of water vapor). It can easily be shown that total mass inside the domain is conserved in the absence of surface precipitation and surface water vapor flux, and that the so-called “precipitation mass sink” effect [studied, for example, by Qiu et al. (1993) and Lackmann and Yablonsky (2004)] is included in this model when using the conservative equation set. We also note that the conservative equation set reduces to the traditional equation set by setting $c_{pv} = c_{vv} = c_l = R_v = \Pi_2 = \Pi_3 = 0$.

The diffusive terms (D) in (1)–(7) are tendencies from a parameterization of unrepresented motions (i.e., turbulence). Our formulation is similar to the one used by RE87, although we utilize the deep anelastic equations (instead of the incompressible Boussinesq equations) during our derivation of these terms. These tendencies are formulated as follows:

$$\begin{aligned} D_u &= \frac{1}{r} \frac{\partial r \tau_{rr}}{\partial r} + \frac{1}{\bar{\rho}} \frac{\partial \bar{\rho} \tau_{rz}}{\partial z} - \frac{\tau_{\phi\phi}}{r}, & D_v &= \frac{1}{r^2} \frac{\partial r^2 \tau_{r\phi}}{\partial r} + \frac{1}{\bar{\rho}} \frac{\partial \bar{\rho} \tau_{z\phi}}{\partial z}, \\ D_w &= \frac{1}{r} \frac{\partial r \tau_{rz}}{\partial r} + \frac{1}{\bar{\rho}} \frac{\partial \bar{\rho} \tau_{zz}}{\partial z}, & D_\chi &= -\frac{1}{r} \frac{\partial r F_r^\chi}{\partial r} - \frac{1}{\bar{\rho}} \frac{\partial \bar{\rho} F_z^\chi}{\partial z}, \end{aligned} \quad (14)$$

wherein χ represents one of the model’s scalars (θ , q_v , or q_l). The stresses (τ) and fluxes (F) are parameterized as in RE87 (p. 545 for the model’s interior, and p. 547 for the surface). Assuming steady, homogeneous turbulence, we derive a turbulence kinetic energy budget for these equations,

$$\nu_h S_h^2 + \nu_v S_v^2 - \nu_v N_m^2 = \epsilon, \quad (15)$$

wherein ν is an eddy viscosity, subscripts h and v refer to effects from unrepresented horizontal and vertical eddy fluxes respectively, N_m^2 is the squared Brunt-Väisälä frequency, ϵ is the rate of dissipation of kinetic energy at molecular scales, and S^2 is deformation given by

$$\begin{aligned} S_h^2 &= 2 \left(\frac{\partial u}{\partial r} \right)^2 + 2 \left(\frac{u}{r} \right)^2 + \left(\frac{\partial v}{\partial r} - \frac{v}{r} \right)^2, \\ S_v^2 &= 2 \left(\frac{\partial w}{\partial z} \right)^2 + \left(\frac{\partial u}{\partial z} + \frac{\partial w}{\partial r} \right)^2 + \left(\frac{\partial v}{\partial z} \right)^2. \end{aligned} \quad (16)$$

We split the dissipation into two components: one accounting for dissipation of horizontal turbulence motions (ϵ_h), and one accounting for dissipation of vertical turbulence motions

(ϵ_v). As did RE87, we assume on dimensional grounds that $\epsilon_h = \nu_h^3/l_h^4$ and $\epsilon_v = \nu_v^3/l_v^4$, wherein l_h and l_v are length scales of the most energetic turbulent motions (that is, the energy-containing eddies). From these assumptions, we derive the diagnostic formulas for eddy viscosity

$$\nu_h = l_h^2 S_h, \quad \nu_v = l_v^2 (S_v^2 - N_m^2)^{1/2}. \quad (17)$$

We set $\nu_v = 0$ if $(S_v^2 - N_m^2) < 0$ (that is, if the Richardson number is greater than unity).

The formulation of N_m^2 for unsaturated air is given by $N_m^2 = (g/\theta_v)\partial\theta_v/\partial z$ and for saturated air is given by

$$N_m^2 = \frac{g}{T} \left(\frac{\partial T}{\partial z} + \Gamma_m \right) \left(1 + \frac{T}{R_d/R_v + q_s} \frac{\partial q_s}{\partial T} \right) - \frac{g}{1 + q_t} \frac{\partial q_t}{\partial z} \quad (18)$$

wherein q_s is the mixing ratio at saturated equilibrium, and Γ_m is the moist-adiabatic lapse rate, which for the conservative equation set is

$$\Gamma_m = g(1 + q_t) \left(\frac{1 + L_v q_s / R_d T}{c_{pm} + L_v \partial q_s / \partial T} \right). \quad (19)$$

To improve energy conservation, dissipative heating can be included in this model. This effect is excluded in most nonhydrostatic numerical models (including the RE87 Model), and this option is available herein by setting $\epsilon = 0$ in (4)–(5). To include this effect with the traditional equation set we use $\Theta_3 = 1/(c_p \pi)$ and for the conservative equation set we use $\Theta_3 = c_v/(c_p c_{vm} \pi)$. For ϵ , we use the turbulence kinetic energy balance equation, (15), for the interior of the model domain. At the surface, we utilize the specifications for surface stress and surface fluxes and, using the same assumptions as Bister and Emanuel (1998), we find the dissipation rate at the surface is

$$\epsilon(z=0) = \frac{2C_D}{\Delta z} (u_1^2 + v_1^2)^{3/2} + g \left[\frac{F_z^\theta}{\theta} + \left(\frac{R_v}{R_d} - 1 \right) F_z^{qv} \right], \quad (20)$$

wherein C_D is the drag coefficient, Δz is the vertical grid spacing, u_1 and v_1 are respectively

the radial and azimuthal velocities at the lowest model level, and F_z^θ and $F_z^{q_v}$ are the surface fluxes for θ and q_v respectively. Our formulation for dissipation rate is slightly different from that in previous studies (e.g., Bister and Emanuel 1998; Zhang and Altshuler 1999) because we account for the buoyancy flux [third term on the left side of (15) and the second term of (20)], which typically increases ϵ in tropical cyclone eyewalls.

The only significant term associated with energy conservation that has been excluded from this model is one related to sedimentation of liquid water entropy [e.g., last term on the right side of (4.6) in Ooyama (2001)]. This term is excluded herein, which is a traditional assumption in numerical models, because of uncertainties about the best way to formulate the term realistically and yet be computationally efficient [see, e.g., Walko et al. (2000) for a discussion of the difficulty in incorporating this effect realistically]. We are currently investigating this effect further, and plan to report our findings in a future study.

b. Numerical methods

The time integration scheme is third-order Runge-Kutta using split-explicit integration for the acoustic modes, following Wicker and Skamarock (2002). To improve the stability and accuracy of the split-explicit time integration method, we include a weak three-dimensional divergence damper on the acoustic time steps, and we integrate θ on the small timesteps, following Skamarock and Klemp (1992).

We write the advection terms in flux form for a variable α as follows:

$$u \frac{\partial \alpha}{\partial r} + w \frac{\partial \alpha}{\partial z} \equiv \frac{1}{r} \frac{\partial (ru\alpha)}{\partial r} + \frac{1}{\bar{\rho}} \frac{\partial (\bar{\rho}w\alpha)}{\partial z} - \alpha \left(\frac{1}{r} \frac{\partial (ru)}{\partial r} + \frac{1}{\bar{\rho}} \frac{\partial (\bar{\rho}w)}{\partial z} \right). \quad (21)$$

The first two terms on the right side are discretized using the fifth-order flux-form scheme by Wicker and Skamarock (2002). To conserve total water, we apply a positive-definite scheme [described in Bryan et al. (2006)] to the advection of q_v and q_l .

Unlike RE87, we use a closed boundary condition (a rigid wall) at the external lateral

boundary, even though an open boundary condition option is available in this code. As compared to an open boundary condition, which is difficult to constrain over long-term integrations, we find a closed boundary produces more stable (i.e., steady) solutions for long-term (> 10 day) simulations. To prevent reflection of gravity waves, we apply Newtonian damping to u , v , and w near this boundary. By comparing to simulations that use open boundary conditions, we find no significant differences for $t < 10$ days, but generally more steady conditions in simulations with the closed domain for $t > 10$ days.

The method to determine \dot{q}_{cond} was described by Bryan and Fritsch (2002, p. 2920). As shown in their study, this numerical model does not precisely conserve total mass and energy, due partly to numerical reasons. However, for simulations using the conservative equation set, we find the artificial loss of mass and energy to be several orders of magnitude lower than for simulations using the traditional equation set. At the end of the simulations (typically at $t = 12$ days), the artificial loss of mass and energy is less than 0.05% of the initial values.

c. Methodology

The initial conditions are identical to those used by RE87. For the base-state environment, we use their “model-neutral” sounding. For our higher-resolution simulations, we interpolate their thermodynamic profile (dots in Fig. 1) to the new grid (lines in Fig. 1), and conditions below their lowest model level are extrapolated downward, as shown in this figure. The sea surface temperature (T_s) is 26.13 °C for all simulations.

The domain is the same size (1500 km \times 25 km) as that used by RE87. Certain settings in the numerical model are varied, depending on the test being conducted, including: the grid spacing (Δr for the radial direction, Δz for the vertical direction); the timestep (Δt); and *a priori* settings for the turbulence parameterization (specifically, l_h and l_v). A summary of model configurations used in this article is presented in Table 1, and further details are provided at appropriate locations later in the text.

Unless stated otherwise, all simulations use the conservative equation set and include

dissipative heating, and the surface exchange coefficient for entropy (C_E) is equal to that for momentum (C_D). (We reiterate that the surface fluxes and stress are formulated the same way as RE87.) The tendency term in the potential temperature equation that mimics radiative cooling (R) is capped at 2 K day^{-1} following Experiment J by RE87, which is the same methodology used in all simulations by Persing and Montgomery (2003) (hereafter referred to as PM03). For all simulations in this article, the parameterization of microphysical processes is identical to that in RE87, and we use $V_t = 7 \text{ m s}^{-1}$ unless stated otherwise. Ice processes are neglected for the sake of simplicity and because we find they have a small effect on maximum simulated intensity.

In all of our simulations, an approximately steady state is achieved by ~ 6 days into the simulation. We quantify the intensity of the simulated tropical cyclones by v_{\max} , which is the maximum value of v (from any gridpoint in the domain) averaged every timestep between $t = 8 - 12$ days. Typically, v_{\max} is located at the top of the boundary layer (at $\sim 1 \text{ km}$). For other analyses herein, we compute average fields using hourly output from $t = 8 - 12$ days.

We have compared output from this new model to output from the RE87 Model. We find that the RE87 Model produces more intense tropical cyclones (by about 10%, as measured by v_{\max}). Output from our new model also tends to be more steady over time. Details are provided in the Appendix. We attribute these differences primarily to improved governing equations and numerical techniques in the new model.

3 Sensitivity tests

We now present the results from several sensitivity tests. The primary focus is the maximum model-produced intensity (v_{\max}). We reiterate that initial and boundary conditions are identical for *all* simulations herein, so any differences in v_{\max} are attributable to numerical model settings. There are a great number of details in the modeling system that we could examine, and it is not our goal to document all possible sensitivities. We focus in this article

on model settings that exhibit the most sensitivity from our tests, and also on aspects of the numerical model that have uncertain formulations (including the parameterization of unresolved physical processes such as turbulence, air-sea interaction, and certain aspects of microphysics). For the sake of completeness, we list here the model settings we investigated but which had a small effect on v_{\max} , and thus are not discussed further: ice microphysical processes², water conservation (i.e., the use of a positive-definite advection scheme), a larger domain size, the external lateral boundary condition, the size and intensity of the initial vortex, and the “precipitation mass sink” effect [e.g., Qiu et al. (1993); Lackmann and Yablonsky (2004)].

As a simple check on the realism of the model output, we compare v_{\max} to the maximum intensity reported in observational studies. In a study of the Atlantic Ocean, DeMaria and Kaplan (1994) reported a maximum intensity for $T_s = 26$ °C of roughly 50 m s^{-1} . In a study of the Eastern North Pacific, Whitney and Hobgood (1997) reported a maximum intensity of 61.1 m s^{-1} . These values are maximum one-minute-sustained wind speeds near the surface, as listed in best-track datasets. For the numerical model, v_{\max} is a long-term (4-day) averaged value of v using output from any model gridpoint, and maximum v is usually located at the top of the boundary layer (at roughly $z = 1 \text{ km}$). Because of the differences, these observed and model-produced measures of intensity are not directly comparable. We note that v_{\max} tends to be about 20% larger than the wind speed at the top of the surface layer (i.e., at the lowest model level). Kepert (2006a,b) documented a similar profile in v using observations of two strong hurricanes. So, for the sake of fair comparison, we increase the maximum reported intensity by roughly 20%, and we conclude that 70 m s^{-1} is a reasonable estimate for the observation-based analogue to v_{\max} for this sea surface temperature, although we place no significance on small (of order 5 m s^{-1}) differences between this number and v_{\max} .

We defer a comparison with theoretical estimates of maximum intensity to a later article, because there are so many cases to consider, and because of the difficulty in determining an

²We have conducted simulations using the single-moment scheme of Lin et al. (1983) [as modified for hurricane research by Braun and Tao (2000)] and the double-moment scheme of Morrison et al. (2008).

appropriate theoretical value for each simulation. For now, we note that some of the simulations herein produce v_{\max} that is significantly greater (by up to 40%) than the theoretical maximum intensity derived by Emanuel (1986), which is consistent with studies using the RE87 Model [e.g., PM03, Bryan and Rotunno (2008)].

a. Grid spacing

Several studies have shown that numerically simulated intensity increases as the horizontal grid spacing decreases [e.g., Braun and Tao (2000), PM03, Yau et al. (2004), Davis et al. (2008), Hill and Lackmann (2008)], at least for grid spacing ≥ 1 km. Presumably, the ability to better resolve nonhydrostatic processes in the eyewall is the primary reason for this sensitivity.

To determine a nominal grid spacing for this study, we conduct a resolution sensitivity test wherein we decrease the grid spacing incrementally until a converged value for v_{\max} is obtained (that is, until v_{\max} stops changing). For these tests, we configure the model to have minimal diffusion by specifying small values for the turbulence length scales: specifically, we use $l_h = 187.5$ m and $l_v = 50$ m. From these simulations, we find a converged value for v_{\max} of ~ 100 m s⁻¹ and this magnitude is achieved for approximately $\Delta r = 1000$ m and $\Delta z = 250$ m (Table 2); further decreases in either Δr or Δz yield essentially the same intensity. We note that this intensity is significantly larger than the maximum observed value (~ 70 m s⁻¹); we analyze and explain this discrepancy later in this article.

Regarding the horizontal grid spacing, we find, similar to previous studies, that the tropical cyclone becomes more intense as the eyewall becomes smaller and better resolved. For Δr of order 1 km or less, the eyewall is represented by at least 8 grid increments; further decreases in Δr do not change the physical width of the eyewall.

Regarding the vertical grid spacing, we find an increase in intensity as Δz increases for this model.³ In this case, the boundary layer becomes poorly resolved, and becomes

³Results could conceivably be different for other numerical models and/or surface-layer parameterizations.

artificially deeper, for $\Delta z \geq 500$ m.

Based on these results, we use $\Delta r = 1000$ m and $\Delta z = 250$ m for all results hereinafter. Based on further tests (not shown), we find it sufficient to use constant Δr in the inner core region only, with stretched grid spacing beyond. Specifically, we use $\Delta r = 1$ km for $r < 64$ km, and then Δr increases gradually to a maximum value of 16 km at $r = 1500$ km. Comparison against a simulation with $\Delta r = 1$ km everywhere yields the same results, so the stretched grid is used hereinafter to reduce computational expense.

We remind readers that simulations with an axisymmetric numerical model (and any two-dimensional model) cannot explicitly produce realistic turbulence. Rather, the effects of all turbulence must be included via parameterization. (See the discussion by RE87, p. 544, for more details.) Consequently, the grid spacing used herein cannot be expected to produce a converged solution in a three-dimensional numerical model, wherein turbulence is parameterized much differently, and can actually be resolved given sufficient resolution [probably with grid spacing of order 100 m, following the theoretical arguments by Bryan et al. (2003)]. Results by Rotunno et al. (2008) confirm this conclusion.

b. Turbulence length scales

One of the most uncertain aspects of axisymmetric numerical models is the parameterization of unrepresented motions. In addition to unresolved subgrid-scale motions, axisymmetric numerical models cannot resolve any three-dimensional motions, such as mesovortices in the eye/eyewall, boundary-layer roll vortices, upper-level asymmetric outflow jets, vortex Rossby waves, etc. Any non-axisymmetric motions must be viewed as turbulence in an axisymmetric model and must be incorporated through parameterization; see section 2b in RE87 for more details. In this model, turbulence is included via the D terms in (1)–(7). The turbulence closure (described in section 2) allows for these tendencies to be larger when the local deformation is larger and/or when the local static stability is smaller. Additionally, the closure contains two unknown length scales: one for horizontal turbulence processes (l_h),

and one for vertical turbulence processes (l_v). The D terms are proportional to l_h and l_v , which are specified *a priori* in this model.

There is no quantitative theoretical guidance for how to set l_h and l_v in an axisymmetric model. RE87 used $l_h = 3000$ m and $l_v = 200$ m in their simulations, which they determined by trial-and-error, and by subjective evaluation of model output. PM03 used $l_h = 750$ m and $l_v = 200$ m for their standard “4x” setup. A different value for l_h was used by PM03 because the RE87 Model’s code specifies l_h in terms of a coefficient times the radial grid spacing (specifically, as $0.2 \times \Delta r$), and PM03 used smaller Δr as compared to RE87. Consequently, without any compensating change in the coefficient, RE87’s code has a fundamentally different representation of horizontal turbulence effects as Δr changes, wherein the turbulent tendencies are *decreased* with higher resolution. However, l_h should be interpreted as a physical parameter in axisymmetric numerical models, because three-dimensional turbulent motions cannot be resolved at *any* grid spacing; thus, the turbulence length scales should be kept constant for resolution sensitivity tests (as was done in the previous subsection).

Here, we evaluate the sensitivity of v_{\max} to l_h and l_v using fixed model parameters (listed as “Default” in Table 1). Results, in terms of v_{\max} , are shown in Fig. 2. There is a strong sensitivity to l_h , but essentially no sensitivity to l_v . For $l_v = 200$ m (the value used by both RE87 and PM03), there is nearly a factor of two increase in v_{\max} when l_h is decreased from 3000 m (the value used by RE87) to 750 m (the value used by PM03). A similar response to changes in l_h and l_v (for fixed grid spacing) was reported by PM03 (in their Table 3).

We find from analysis of tendencies in the model’s governing equations (not shown) that with l_h less than ~ 1000 m the tendency from horizontal turbulence is negligible compared to other terms in the governing equations. So, as $l_h \rightarrow 0$ the flow becomes essentially inviscid (in the radial direction). To investigate the effects of a truly inviscid model setup, we conduct additional simulations with further decreases in l_h , including $l_h = 0$. Results show that v_{\max} (solid line in Fig. 3) asymptotically approaches 113 m s^{-1} as $l_h \rightarrow 0$. For our default model setup, there is additionally a flow- and scale-dependent numerical diffusion that is inherent

to the fifth-order advection scheme used herein; this term prevents features from collapsing to a scale smaller than ~ 6 times the grid length. To check the effects of this diffusive term, we also ran a set of simulations (not shown) that uses sixth-order advection, which has no implicit diffusion; these simulation have the same response, although v_{\max} asymptotically approaches a slightly lower value (103 m s^{-1}).

These results are somewhat similar to results in Emanuel (1989), who used a balanced axisymmetric model expressed in angular momentum coordinates. Starting with very small diffusion in the lateral direction (his experiment C1), he found essentially no change in v_{\max} for a factor of three increase in l_h (his experiment A), and a slight ($\sim 10\%$) decrease in v_{\max} for a further factor of three increase in l_h (his experiment C2) (see Fig. 5 in his article). The same behavior is seen in our model for $l_h \approx 100 \text{ m}$. Emanuel (2008, personal communication) has found that further decreases in l_h (to near zero) in his model result in a slight decrease in v_{\max} , although this may be attributable to numerical problems with low diffusion or to other differences in these two models.

What is notably different from the results reported by Emanuel (1989) is the maximum intensity, which is near the theoretical PI ($\sim 60 \text{ m s}^{-1}$) in his study. In our case, PI is also roughly 60 m s^{-1} (see PM03), but v_{\max} significantly exceeds this value when $l_h < 3000 \text{ m}$. This ability to significantly exceed the theoretical PI for small l_h appears to be related primarily to the existence of unbalanced flow (which is not possible in Emanuel’s model). In our model, we find that v_{\max} is close to the maximum gradient wind speed ($v_{g,\max}$) for $l_h > 1500 \text{ m}$ (Fig. 3), but v_{\max} notably exceeds $v_{g,\max}$ as lateral diffusion becomes small. Because of the complexity of this issue, we will address it in a separate article.

Of more interest to this study is that v_{\max} greatly exceeds the maximum value that has ever been observed for this environment ($\sim 70 \text{ m s}^{-1}$, see beginning of section 3). This only happens in our model when l_h is small, i.e., when the flow is essentially inviscid in the radial direction. To understand this result further, we note that radial gradients of all model fields are strongly affected by l_h . Specifically, larger l_h increases the turbulent diffusion, which

yields weaker radial gradients (in both scalar and velocity fields). For example, we show in Fig. 4 the angular momentum ($M \equiv rv + fr^2/2$) and the pseudoadiabatic equivalent potential temperature (θ_e) (Bryan 2008) at the top of the boundary layer. The large differences in θ_e in the eye of these simulations (that is, for $r < 10$ km in Fig. 4b) are not relevant to the maximum intensity in these simulations, as discussed below. More important are the radial gradients near the location of v_{\max} (dots in Fig. 4), which are largest for small values of l_h ; this is because the eyewall of hurricanes is strongly frontogenetic, as discussed by Emanuel (1997). For small l_h , this frontogenetic zone collapses to a small scale (approximately 8 km wide). But the diffusion terms are frontolytic; thus, as l_h is increased, and lateral diffusion becomes a significant term in the governing equations, the diffusive terms produce weaker gradients in both scalars and momentum⁴ (Fig. 4). Consequently, with large l_h , M from the environment has not been drawn as far into the center of circulation as it can be with smaller l_h , and thus v_{\max} is smaller. The weaker radial gradients of scalars are also consistent with weaker intensity because of approximate thermal-wind balance; that is, because $v \approx 0$ at the top of the troposphere, then weaker shear (consistent with a weaker radial gradient in entropy by thermal wind) must mean weaker intensity.

Based on the preceding arguments, one might wonder whether further increases in resolution would lead to even greater v_{\max} , because even larger gradients in M and θ_e could be resolved. Our sensitivity studies do not support such a conclusion. Using $l_h = 0$, v_{\max} is essentially the same for any $\Delta r < 4$ km (Table 3). In fact, we find that the width of the eyewall, and hence the width of the frontogenetic zone, converges to ~ 8 km for $\Delta r < 4$ km (Table 3, where the eyewall is defined as $w \geq 0.5$ m s⁻¹). The processes that prevent the eyewall from collapsing to an infinitesimal scale (as might be expected for zero turbulent diffusion in a frontogenetical zone) would be an interesting topic for future study, although we surmise that the finite depth of the boundary layer in this model likely plays a role in dictating this finite updraft width.

⁴The same tendency has been found in three-dimensional simulations that explicitly resolve asymmetries; see, e.g., Wang (2002b), Wu and Braun (2004), and Yang et al. (2007).

To help explain why v_{\max} is bounded in our simulations, we draw upon the analytic study of tropical cyclone structure and intensity by Emanuel (1986). By assuming gradient-wind balance, hydrostatic balance, and moist slantwise neutrality in the free atmosphere, Emanuel (1986) derived a relationship between the radial gradient of moist entropy (s) and the radial gradient of M in the eyewall [see his (13)]. If we assume that both s and M could collapse to discontinuities in the frontogenetic region of the eyewall, then we can integrate Emanuel’s (13) across the discontinuities, which yields

$$v_{g,\max}^2 = -2(T_B - T_{\text{out}})\Delta s, \quad (22)$$

which is valid only in the eyewall (at the radius of maximum winds), wherein Δs is the change in s across the discontinuity, T_B is temperature at the location of $v_{g,\max}$, and T_{out} is the “outflow temperature” [which is the temperature, at large radius, along a trajectory that passes through $v_{g,\max}$ (see Bister and Emanuel 1998, p. 237)]. The important conclusion to be drawn from (22) is that $v_{g,\max}$ must be finite because Δs must be finite. Using estimated values of T_B , T_{out} , and Δs from our weak-diffusion simulations, (22) predicts $v_{g,\max} \approx 100 \text{ m s}^{-1}$, which is consistent with $v_{g,\max}$ from these simulations (Fig. 3). One might wonder what limits the value of Δs , and thus what ultimately limits $v_{g,\max}$; this could be addressed in a future study of theoretical PI.

Returning now to the dependence of model-simulated v_{\max} on l_h , our analysis probably explains other simulations of very intense tropical cyclones with axisymmetric numerical models. For example, Hausman et al. (2006) report v_{\max} exceeding 130 m s^{-1} for $T_s = 28 \text{ }^\circ\text{C}$. [The maximum observed surface winds for $T_s = 28 \text{ }^\circ\text{C}$ in the study by DeMaria and Kaplan (1994) was $\sim 70 \text{ m s}^{-1}$.] Hausman et al. (2006) had no parameterization for horizontal turbulence in their model (other than the implicit filter in their model’s numerics, which is similar to the high-order diffusion used in our model). Their results are consistent with ours, in the sense that essentially inviscid flow leads to very large intensities that are much greater

than observed maximum intensities.

Our analysis also explains why PM03 found an increase in intensity with decreasing grid spacing using the RE87 Model. As discussed at the beginning of this subsection, their changes in Δr were accompanied by changes in l_h , the latter of which we find is important for maximum simulated intensity. In contrast, PM03 implicated the existence of high-entropy air in the low-level eye (e.g., $r < 10$ km in Fig. 4b); this feature has since been shown to be unimportant for maximum intensity in axisymmetric numerical models [see Bryan and Rotunno (2008) for a detailed analysis], and is thus not discussed further herein.

One might wonder whether horizontal diffusion of scalars or momentum is more important for changes in v_{\max} . To investigate, we conduct a series of simulations that calculate different horizontal eddy viscosities for scalars and momentum using a specified horizontal length scale for scalars (l_h^s) and one for momentum (l_h^m). From a broad set of simulations (not shown here, due to space limitations), we find that *both* horizontal diffusion of scalars and momentum is important. If one of these length scales is fixed, and the other is decreased gradually to zero, we again find that v_{\max} asymptotically approaches a constant, although this constant is different for each experiment. Overall, we find that v_{\max} is *more sensitive* to changes in l_h^m than to changes in l_h^s , although we reiterate that v_{\max} is sensitive to changes in either length scale.

Before proceeding to other sensitivities in this numerical model, we briefly investigate the hurricane structure as the turbulence coefficients are changed. We show in Fig. 5 the azimuthal and radial flow fields from simulations with three different configurations for turbulence. For relatively large l_h and l_v (Fig. 5a), the value of v_{\max} is 48 m s^{-1} , which is less than our estimate for observed maximum intensity (70 m s^{-1}). The maximum value of radial inflow is 12 m s^{-1} , which is comparable to values reported in observed tropical cyclones (e.g., LeeJoice 2000). Overall, for these settings, the model produces features that are reasonably consistent with observational analyses of strong tropical cyclones.

Using smaller l_h , but the same l_v (Fig. 5b), the model yields a much smaller radius of

maximum winds (as compared to that from the previous model setting). In this case, v_{\max} is 86 m s^{-1} , which is notably larger than our estimate for observed maximum intensity (70 m s^{-1}); the large discrepancy ($\sim 15 \text{ m s}^{-1}$) raises concerns about the realism of this simulation. Furthermore, consistent with larger values of azimuthal velocities, the maximum value of radial inflow is also larger. In this case, the maximum value of radial inflow is $\sim 25 \text{ m s}^{-1}$, which is about twice as large as any value reported by LeeJoice (2000), but is comparable to observations of intense tropical cyclones by Bell and Montgomery (2008) and Kepert (2006a,b). The total depth of radial inflow is $\sim 2 \text{ km}$ in this simulation, which is slightly higher than, although comparable to, the structure documented in these observational studies. Overall, the structures produced by this model setting can be characterized as extreme, and perhaps unrealistic (at least for v_{\max}), compared to available observations.

Using the same (small) value of l_h , but much smaller l_v , the maximum azimuthal velocity and the radius of maximum winds remain essentially unchanged (Fig. 5c). However, the depth of the radial inflow is much smaller compared to the previous case. Furthermore, the magnitude of maximum radial inflow is 40 m s^{-1} , which is much higher than has been shown in the observational studies cited above. A strong radial *outflow* ($> 20 \text{ m s}^{-1}$) exists at $z \approx 1.5 \text{ km}$, which is also much greater than has been previously documented (e.g., Bell and Montgomery 2008). These structures are clearly not representative of natural tropical cyclones. In some simulations with low l_h and l_v (although not in this case), inertial instability exists in the eyewall, which is another unnatural feature that can develop in weak-turbulence simulations.

To summarize, the intensity *and* structure of tropical cyclones in axisymmetric numerical models is very sensitive to the specification of turbulence intensity. This means that large uncertainty is an inherent characteristic of axisymmetric numerical model simulations, considering that there is currently no quantitative theoretical guidance with which to specify turbulence effects (particularly in the radial direction). Our analysis further reveals that unnatural features may be produced in an axisymmetric model. As an example, v_{\max} of

113 m s⁻¹ (Fig. 3) is clearly unnaturally high as compared to the maximum observed intensity for this sea-surface temperature (~ 70 m s⁻¹). Consistent with such large azimuthal velocities are unnaturally large values of radial inflow (e.g., $|u| > 40$ m s⁻¹).

Based on these results, we conclude that nearly inviscid axisymmetric model setups (i.e., $l_h \rightarrow 0$) cannot reproduce realistic tropical cyclones. Furthermore, if l_h is set to a moderately large value (e.g., 3000 m, which was used by RE87), then no other setup of the numerical model that has been studied herein yields an intensity larger than the climatologically observed maximum of ~ 70 m s⁻¹.

It follows that turbulence in the radial direction limits axisymmetric tropical cyclone intensity. As discussed earlier, this is because turbulent diffusion weakens the radial gradient of angular momentum in the eyewall (which prevents large values of environmental angular momentum from being drawn to small radius) and also weakens radial gradients of scalars (which consistently means weaker intensity by consideration of thermal-wind balance). Further analysis with three-dimensional models are needed to verify these conclusions, particularly because realistic three-dimensional turbulent flows (e.g., eye/eyewall mesovortices, boundary-layer roll vortices, upper-level asymmetric outflow jets, etc) may act differently than the way they are parameterized in this model.

One might wonder whether we can determine values for l_h and l_v that yield reasonably realistic hurricanes as compared to observations. Based on the estimated observed maximum intensity of 70 m s⁻¹, as well as comparisons of maximum radial inflow to observations, it seems that $l_h \approx 1500$ m and $l_v \approx 100$ m are appropriate. Additionally, observations of azimuthally average properties can be useful in this regards. In an analysis of a category-5 tropical cyclone, Montgomery et al. (2006) found the radial gradient of moist entropy in the eyewall to be -1.7×10^{-3} m s⁻² K⁻¹; the same value occurs in our simulations if $l_h = 1500$ m. Despite this encouraging comparison between model output and observations, we cannot say with confidence that these values of l_h and l_v will be appropriate for all cases.

As discussed in section 1, a primary goal of this study is to identify the model settings

that allow for *maximum possible* intensity in numerical models. Small values of l_h clearly lead to this goal. Thus, we retain small values of l_h for sensitivity tests that follow, although we also present results with $l_h = 1500$ m as a likely appropriate setting for comparison against observations.

c. Ratio of surface exchange coefficients

Numerical simulations (e.g., Rosenthal 1971; Braun and Tao 2000) and theoretical analysis (e.g., Emanuel 1986, 1995) have demonstrated a large sensitivity of maximum intensity to the ratio of surface exchange coefficients for entropy and momentum (C_E/C_D). Observational studies have found that this ratio varies between roughly 0.5 and 1.5, with the lowest values being appropriate for near-surface wind speeds of ~ 25 m s⁻¹ (e.g., Black et al. 2007). However, an appropriate value for large wind speeds (of order 50 m s⁻¹) remains uncertain.

To investigate this sensitivity in the numerical model, we set $C_E = 1.2 \times 10^{-3}$, based on recent observational studies (e.g., Drennan et al. 2007). Because C_D seems to be a more uncertain parameter (e.g., Powell et al. 2003; French et al. 2007), we vary this parameter across a broad range of values. These lower values of both C_E and C_D (as compared to the default formulations from RE87) result in much slower evolution, and sometimes a steady cyclone does not develop by $t = 12$ days. Consequently, we double the intensity of the initial vortex (to 30 m s⁻¹) to hasten initial development for this sensitivity test. (These changes to C_E , C_D , and initial vortex intensity were made for this subsection only.) Results for C_E/C_D between 0.25 and 2 are shown in Fig. 6.

Under the assumption of inviscid flow above the boundary layer, Emanuel (1986, 1995) derived a theoretical relationship, $v_{\max} \sim (C_E/C_D)^{1/2}$. For a low value of l_h in the numerical model (solid line in Fig. 6), we find a similar result: $v_{\max} \sim (C_E/C_D)^{0.44}$. For even lower values of l_h (not shown), we find even closer correspondence to theory; for $l_h = 94$ m, we find $v_{\max} \sim (C_E/C_D)^{0.53}$. Thus, the model results trend towards the theoretical results as turbulence intensity decreases (i.e., as inviscid flow is approached).

In contrast, with higher values of l_h , v_{\max} shows a clearly different dependence. For $l_h = 1500$ m (dashed line in Fig. 6), v_{\max} varies as $(C_E/C_D)^{0.34}$. For $l_h = 3000$ m (dotted line in Fig. 6), v_{\max} varies as $(C_E/C_D)^{0.31}$ for $C_E/C_D \leq 1.25$ and v_{\max} is independent of C_E/C_D for $C_E/C_D \geq 1.5$. Given that non-zero turbulence is needed in the model to reproduce realistic hurricane structures (see previous subsection), these results suggest that viscous terms are needed for an analytical theory of maximum intensity that is appropriate for natural tropical cyclones. Our results might also explain why Braun and Tao (2000) did not find close correspondence between their high-resolution three-dimensional simulations and Emanuel’s theoretical model; that is, turbulent diffusion in their model (resolved and/or parameterized) must be relatively important.

As discussed earlier, the approximate maximum intensity of observed tropical cyclones is roughly 70 m s^{-1} for this environment. For $l_h = 375$ m, C_E/C_D needs to be less than 0.5 to match this intensity; this seems too low compared to observed values (e.g., Powell et al. 2003; Black et al. 2007), although it could be argued that such low values have never been observed because of difficulties measuring exchange coefficients in high wind speeds. For $l_h = 1500$ m, v_{\max} matches the maximum observed intensity for $C_E/C_D \approx 0.75$; the same conclusion was drawn by Emanuel (1995). For $l_h = 3000$ m, the model cannot reproduce maximum observed intensity, which suggests that this specification of turbulence intensity is too extreme.

Although the formulation of surface exchange coefficients has been studied often in recent observational campaigns, these results suggest that turbulence in the radial direction is a crucially important parameter that should also be studied further. Indeed, assuming $l_h = 1500$ m is an appropriate value, then v_{\max} from this model changes by only $\sim 25\%$ if the ratio C_E/C_D is doubled from 0.5 to 1.0 (Fig. 6). In contrast, v_{\max} can change by 100% for values of l_h that have been used in published literature (Fig. 2). Further comparison between model results and observations could be undertaken to help constrain the value of l_h for axisymmetric models. Additional analyses of the axisymmetric structure of intense tropical

cyclones in steady state — such as the analyses presented by Bell and Montgomery (2008) — would be valuable for this purpose. Additionally, a similar study with a three-dimensional numerical model should be conducted to check whether these results are sufficiently general.

d. Liquid water fall velocity

We now investigate sensitivity to the specification of terminal fall velocity for liquid water, V_t . The scheme used herein is the same as that used by RE87, and it is quite simple: if q_l exceeds 1 g kg^{-1} , then this liquid is assumed to fall at V_t , which by default is 7 m s^{-1} . This approach is somewhat unrealistic, but it allows us to document the fundamental response of v_{\max} to the fall velocity of condensate in an easily understandable manner.

Results are shown in Fig. 7 for simulations using $l_h = 375 \text{ m}$ (solid) and $l_h = 1500 \text{ m}$ (dashed). We note that this model’s governing equations allow for exact reversible thermodynamics when $V_t = 0$ (in the absence of turbulence effects). This capability is not available in most atmospheric numerical models, which typically neglect terms in the thermodynamical equation (see Bryan and Fritsch 2002).

For reversible thermodynamics ($V_t = 0$), the weakest intensity is produced. As V_t is increased, v_{\max} increases, and the intensity for large V_t is about 60% larger than the reversible case. We also ran simulations (not shown) in which condensate is immediately removed from the atmosphere when q_l exceeds 1 g kg^{-1} ; this is analogous to a pseudoadiabatic process, in which condensate is assumed to immediately fall out from air parcels upon formation. In these latter simulations, v_{\max} is the same as simulations with large V_t (Fig. 7).

These results are generally consistent with those from previous studies [e.g., Wang (2002a), Hausman et al. (2006)], in the sense that larger fall velocities yield greater intensities. We have also conducted simulations (not shown) with more complex specifications for terminal fall velocity in which V_t varies proportionally to q_l , and also simulations that incorporate ice microphysics. From these simulations, we draw the same overall conclusion concerning the correlation between v_{\max} and V_t (in which we use a characteristic value of V_t , such as an

average value in the eyewall).

A qualitative consideration of buoyancy helps explain this result. Specifically, larger (positive) buoyancy in a column yields lower perturbation pressure at the bottom of the column⁵; stronger near-surface winds are, of course, consistent with lower pressure. In the simulations with small V_t , there is a great deal of condensate in the column, which contributes to lower buoyancy, and is thus consistent with weaker intensity. For $V_t \rightarrow \infty$, there is no condensate in the column, and thus buoyancy is comparatively higher, which is consistent with stronger intensity. This line of reasoning is supported by the analytic study by Emanuel (1988), who found that an assumption of pseudoadiabatic thermodynamics ($V_t \rightarrow \infty$) yielded much stronger tropical cyclones (by ~ 25 mb, in terms of minimum central pressure) than an assumption of reversible thermodynamics ($V_t = 0$). Emanuel (1988) similarly concluded that water loading plays a key role in reducing the intensity in the reversible case.

To provide further guidance for the development and evaluation of PI theories, we examine the total moist entropy (s) from our simulations. In the absence of turbulence effects, s should be conserved following a parcel. To determine an appropriate mathematical formulation of s , a further assumption must be made about the liquid water fall velocity. On one extreme, assuming $V_t = 0$, an exact expression for s in reversible conditions — hereinafter referred to as s_r — can be derived,

$$s_r = (c_p + c_l r_t) \ln T - R_d \ln p_d + \frac{L_v q_v}{T} - R_v q_v \ln(\mathcal{H}), \quad (23)$$

(e.g., Emanuel 1994) wherein \mathcal{H} is relative humidity and p_d is the partial pressure of dry air. On the other extreme, if liquid water is immediately removed upon formation (that is, for $V_t \rightarrow \infty$), then a highly accurate expression for s in pseudoadiabatic conditions —

⁵This statement follows from both the hydrostatic equation and from a nonhydrostatic anelastic pressure equation of form $\nabla^2 \pi' = \partial B / \partial z$.

hereinafter referred to as s_p — can be derived

$$s_p = c_p \ln T - R_d \ln p_d + \frac{L_0 q_v}{T} - R_v q_v \ln(\mathcal{H}), \quad (24)$$

(Bryan 2008) wherein $L_0 = 2.555 \times 10^6 \text{ J kg}^{-1}$ is a constant.

We show the distribution of s for three simulations in Fig. 8, wherein s_r is shown on the left and s_p is shown on the right. In all panels, the trajectory for the parcel that passes through v_{\max} is shown as a thick line. As expected, s_r is approximately conserved in the free atmosphere (i.e., above the boundary layer) in the simulation with $V_t = 0$ (Fig. 8a), as revealed by the near equivalence of the trajectory and a contour of s_r . In contrast, s_p is clearly not conserved in this case (Fig. 8b), especially when the parcel reaches mid levels and q_l is relatively large. For $V_t = 7 \text{ m s}^{-1}$ (which is the value used by RE87 and PM03), neither s_r nor s_p are conserved following a parcel (Fig. 8c–d). Consequently, this case would be difficult to analyze analytically, because neither the reversible nor the pseudoadiabatic assumption is truly applicable. For $V_t = 20 \text{ m s}^{-1}$, s_r is clearly not conserved following a parcel, as expected (Fig. 8e); however, s_p is conserved well along the trajectory (Fig. 8f), indicating that liquid water is removed sufficiently quickly such that the pseudoadiabatic assumption can be invoked for this case.

These examples reveal that a thermodynamical constraint that is suitable for analytical study can probably only be made for one of the extreme situations (i.e., either reversible or pseudoadiabatic thermodynamics): it seems unlikely that a conserved variable could be formulated for the $V_t = 7 \text{ m s}^{-1}$ case. If the goal is to study the maximum possible intensity of tropical cyclones, then clearly the pseudoadiabatic assumption should be made. Of course, this state would never be realized in natural tropical cyclones, because the fall velocity of condensate is of order 5 m s^{-1} (for liquid condensate, but smaller for snow). Consequently, there is a dilemma that is analogous to the choice for turbulence intensity (section 3b); that is, the pseudoadiabatic assumption may yield the *maximum possible* intensity, but this

assumption is clearly not appropriate for natural tropical cyclones.

One might wonder whether the environmental sounding used for these simulations has some affect on these results. The sounding used herein was generated by RE87 to be approximately neutral to convection in their modeling study. With the different governing equations and resolution of this model, it is conceivable that a different result might be obtained for a truly moist-neutral sounding appropriate for our model. Furthermore, by changing the physics of the model from reversible ($V_t = 0$) to pseudoadiabatic ($V_t \rightarrow \infty$), the fixed model atmosphere is clearly no longer neutral to convection across these tests. To investigate, we create two exactly moist-neutral soundings using the model's equations: one for the reversible case (solid line in Fig. 9) and one for the pseudoadiabatic case (dashed line in Fig. 9). Both soundings have exactly zero CAPE under their respective thermodynamical assumption. To be as comparable as possible to the control simulations, we set the surface θ_e to be identical to that in the control sounding, and we use a similar tropopause height (15 km). Results using $l_h = 375$ m are listed in Table 4. Overall, the same conclusion is obtained: reversible thermodynamics yields the weakest intensity, and pseudoadiabatic thermodynamics yields the strongest intensity, although for these new soundings the difference is greater. We are unsure, at this time, why the difference in intensity is much larger than that found by theoretical estimates (e.g., Emanuel 1988), which could be a topic for future study.

Finally, we note that these results reveal potential implications for intensity change forecasting, as well as for NWP model development. Specifically, modest changes in V_t can result in significant changes in tropical cyclone intensity. This is especially the case for $V_t < 5$ m s⁻¹ (Fig. 7) wherein a change in V_t of only 1 m s⁻¹ leads to a change in intensity of $\sim 10\%$. Consequently, from a physical perspective, changes in the aerosol content of a tropical cyclone's environment should change V_t , which might then lead to significant ($\sim 10\%$) changes in intensity. These microphysical aspects of tropical cyclones might be part of the reason why tropical cyclone intensity has been so difficult to predict operationally.

e. Equation set

One unique aspect of this numerical model is the equation set, which mathematically conserves internal energy for reversible moist flows. In contrast, most nonhydrostatic cloud-scale models use an approximate equation set wherein the heat capacities of water are neglected, which leads to a cold bias when the liquid water content is large (Bryan and Fritsch 2002). For numerical models that do include these effects (e.g., Ooyama 2001; Satoh 2003), it is unclear whether simulations of tropical cyclones are considerably different from simulations that use traditional approximate equation sets. Therefore, in this subsection we investigate the impacts of the different equation sets in our model.

Fig. 10 shows a comparison of v_{\max} from simulations that use the conservative equation set (solid lines) and simulations that use the traditional equation set (dashed lines). For relatively large fall velocity ($V_t > 5 \text{ m s}^{-1}$), there is essentially no difference in results. This is because the derivation of the traditional equation set is analogous to making the pseudoadiabatic assumption, wherein liquid water contents are low and thus the heat content of liquid water can be neglected (Bryan 2008). In contrast, for relatively small fall velocity ($V_t < 5 \text{ m s}^{-1}$), the simulations using the traditional equation set are 10–20% weaker than simulations using the conservative equation set. This result is consistent with the arguments provided in the previous subsection; that is, lower column-integrated buoyancy yields weaker intensities. In this case, the cool bias incurred by neglecting the specific heats of water leads to the weaker intensities.

4 Summary

In this study, we use an axisymmetric model to investigate the maximum possible intensity of numerically simulated tropical cyclones. The model is designed to conserve total mass and energy in reversible saturated conditions, and uses relatively newly developed numerical techniques. Compared to the axisymmetric model developed by Rotunno and

Emanuel (1987), tropical cyclones in the new model are systematically weaker by $\sim 10\%$ (see Appendix); this difference is attributed to several approximations made in the Rotunno-Emanuel model.

Sensitivity tests are conducted to determine the model setup that yields maximum sustained azimuthal velocity (v_{\max}), and to determine the sensitivity of v_{\max} to uncertain aspects of the model system. Based on a large set of simulations, we find maximum intensity occurs with the following model setup:

- $\Delta r \approx 1$ km or less and $\Delta z \approx 250$ m or less;
- inviscid flow in the radial direction;
- pseudoadiabatic thermodynamics (i.e., hydrometeor fall velocities greater than ~ 10 m s $^{-1}$);
- an equation set that conserves internal energy (if hydrometeor fall velocities are of order 1 m s $^{-1}$).

These findings should be useful for development of analytical models of maximum intensity. However, we note that some of these model settings yield unnatural structures, as compared to available observations of axisymmetric tropical cyclone structure. For example, the simulations with essentially inviscid flow produce inflow velocities and azimuthal velocities that have never been documented with observations; the maximum azimuthal velocity exceeds 110 m s $^{-1}$, which is much greater than the maximum observed value (~ 70 m s $^{-1}$) for this environment. Thus, some of these settings are clearly unnatural. Indeed, it is quite obvious that natural tropical cyclones are not inviscid, and that pseudoadiabatic thermodynamics are not applicable. This poses a problem for development of analytic models of maximum intensity, because the governing equations for such extreme assumptions are the most simple, and thus most tractable, for analytic development.

The intensity and structure of the simulated tropical cyclones is *most* sensitive to the specification of turbulence intensity. In particular, turbulence in the radial direction limits

maximum intensity because it reduces the radial gradient of angular momentum in the eyewall (which prevents large values of environmental angular momentum from being drawn to small radius) and turbulence also reduces radial gradients of scalars (which is consistent with weaker intensity, owing to approximate thermal wind balance). Unfortunately, the parameterization of turbulence is the most uncertain aspect of axisymmetric models; there is no theory for how to formulate the intensity of turbulence in this framework, and few observations are available to constrain the adjustable settings (e.g., l_h and l_v) in the model of turbulence used herein. Based on a cursory comparison to observations, we find that $l_h \approx 1500$ m and $l_v \approx 100$ m are reasonable settings. Additional high-resolution observations within the eyewall of steady tropical cyclones, such as those presented by Bell and Montgomery (2008), would be needed to gain more confidence in these turbulence settings.

An analytic model that assumes inviscid flow above the boundary layer (Emanuel 1986, 1995) found that maximum intensity is proportional to the ratio of surface exchange coefficients for entropy and momentum: $v_{\max} \sim (C_E/C_D)^{1/2}$. This result is approximately reproduced for the essentially inviscid model setup. However, for greater intensity of turbulence, the model-produced v_{\max} shows less sensitivity to C_E/C_D . These results suggest that the ratio C_E/C_D might be less important to tropical cyclone intensity than previous studies have suggested.

Finally, it seems possible that the difficulty in real-time forecasts of intensity may be partly related to the specification of turbulence in NWP models and/or the general lack of understanding of turbulence effects in hurricanes. We recommend an examination of turbulence parameterizations in NWP models as a possible fruitful avenue of research. However, three-dimensional large eddy simulation (LES), such as that conducted by Rotunno et al. (2008), might be needed to fully understand the effects of turbulence on hurricane intensity, because high-resolution LES is insensitive (in principle) to modest changes in the subgrid

turbulence parameterization.

Acknowledgments. The authors thank Chris Davis, Greg Holland, and Morris Weisman for providing reviews of an earlier version of this manuscript, and Kerry Emanuel, Yuqing Wang, and an anonymous reviewer for their formal reviews of this manuscript. All figures were created using the Grid Analysis and Display System (GrADS).

APPENDIX

Comparison with the RE87 Model

Here we compare results from the new model (hereafter referred to as the BR Model) to results from the RE87 Model. This comparison helps put the new model's results into context with previously published results [e.g., RE87, Bister and Emanuel (1998), PM03], and it also serves as a cursory check of the model's accuracy. For these tests, we use two settings: 1) the settings used by RE87, hereinafter referred to as the 1x configuration; and 2) the settings used in the 4x simulations by PM03, wherein grid spacing (in both directions) is reduced by a factor of four, timestep is reduced by a factor of four, and l_h is reduced by a factor of four, compared to the 1x configuration (see Table 1). We use $V_t = 7 \text{ m s}^{-1}$ for all simulations (as in RE87). For simulations with the BR Model we use the conservative equation set, although for this value of V_t the impact of this different equation set is minimal (Fig. 10). We neglect dissipative heating for these tests because it is not included in the RE87 Model. Consequently, these tests primarily evaluate the differences that are attributable to numerical techniques and other seemingly minor differences, as explained below.

Time series of v_{\max} (Fig. A1) reveal two primary differences in model output. First, the BR Model generally produces solutions that are steadier for a longer period of time, whereas the RE87 Model output drifts more noticeably after roughly 10 days. In this case, the RE87 Model output drifts upward with the 1x configuration, but drifts downward with the 4x configuration; the same general result was documented by Persing and Montgomery (2005). A slight weakening trend occurs with the BR Model, especially for the 4x setup; however, with the 4x configuration, the downward trend between days 8–16 is a factor of two smaller than with the RE87 Model. We attribute the steadier solutions to improvements in the BR Model, particularly with regards to mass conservation and the more accurate numerical techniques, but also to the different lateral boundary condition (discussed in section 2b).

The second primary difference is weaker intensities with the BR Model (Fig. A1). Overall, v_{\max} from the BR Model is about 10% smaller than v_{\max} from the RE87 Model. This

result is difficult to explain. To gain insight, we ran a multitude of test simulations with the BR Model using the 4x configuration in which we modified the governing equations, numerical techniques, and physical constants to be like those in the RE87 Model in an attempt to reproduce the greater intensity. We made too many changes to document in detail herein. Overall, we find that *some* changes to the BR Model caused slightly weaker intensities, but that *most* changes we investigated caused slightly stronger intensities when implemented into the BR Model. Thus, several approximations in the RE87 Model have small positive contributions to intensity, and that the overall effect is a notable ($\sim 10\%$) positive contribution. To demonstrate, we list three modifications in Table A1 that we made to the BR Model for which we find a notable positive impact on intensity; also listed in this table is v_{\max} when using the unmodified versions of the BR and RE87 Models. For these tests, we use the 4x configuration (Table 1). The changes are explained in the next several paragraphs.

First, we modified only the values of physical constants in the model. The default values for both models are listed in Table A2. We also modified the formulation of the saturation vapor pressure; the RE87 Model uses the formulation from Klemp and Wilhelmson (1978), whereas the BR Model uses the formulation from Bolton (1980). The values/formulations that are default in the BR Model come from more recent references, and thus are believed to be more accurate. In this test, hereinafter referred to as BR-A, we find a small ($+2.2 \text{ m s}^{-1}$) increase in intensity (Table A1).

Second, we modified only the pressure gradient term. (We did not retain the changes from the previous paragraph for this test.) The BR Model uses the unapproximated form, $-c_p \theta_v \nabla \pi'$. The RE87 Model uses a linearization whereby θ_v is replaced by the base-state value, $\bar{\theta}_v$. In this test, hereinafter referred to as BR-B, we find a small ($+1.3 \text{ m s}^{-1}$) but positive increase in intensity (Table A1).

Third, we modified only the formulation of the advection terms to be second-order, instead of fifth-order, although the BR Model uses a flux-form for the advection terms

whereas the RE87 Model uses an advective form. (Again, we did not retain changes from the previous paragraphs.) In this test, hereinafter referred to as BR-C, we find a small (+1.6 m s⁻¹) but positive increase in intensity (Table A1).

When we incorporate all three of these changes in a single test, hereinafter referred to as BR-ABC, we find an intensity increase of +5.3 m s⁻¹ (Table A1), or roughly a 7% increase in intensity. These changes seem to explain most of the discrepancy between the BR Model and the RE87 Model. More generally, we conclude that a series of reasonable approximations, that by themselves may be small and insignificant, can together act to create a more substantial difference in simulated tropical cyclone intensity. We further conclude that several such approximations bias the RE87 Model toward comparatively stronger intensities.

References

- Bell, M. M., and M. T. Montgomery, 2008: Observed structure, evolution, and potential intensity of category 5 Hurricane Isabel (2003) from 12 to 14 September. *Mon. Wea. Rev.*, **136**, 2023–2046.
- Bister, M., and K. A. Emanuel, 1998: Dissipative heating and hurricane intensity. *Meteor. Atmos. Phys.*, **65**, 233–240.
- Black, P. G., E. A. D’Asaro, W. M. Drennan, J. R. French, P. P. Niiler, T. B. Sanford, E. J. Terrill, E. J. Walsh, and J. A. Zhang, 2007: Air-sea exchange in hurricanes: Synthesis of observations from the Coupled Boundary Layer Air-Sea Transfer Experiment. *Bull. Amer. Meteor. Soc.*, **88**, 357–374.
- Bolton, D., 1980: The computation of equivalent potential temperature. *Mon. Wea. Rev.*, **108**, 1046–1053.
- Braun, S. A., and W.-K. Tao, 2000: Sensitivity of high-resolution simulations of Hurricane Bob (1991) to planetary boundary layer parameterizations. *Mon. Wea. Rev.*, **128**, 3941–3961.
- Bryan, G. H., 2008: On the computation of pseudoadiabatic entropy and equivalent potential temperature. *Mon. Wea. Rev.*, in press.
- Bryan, G. H., and J. M. Fritsch, 2002: A benchmark simulation for moist nonhydrostatic numerical models. *Mon. Wea. Rev.*, **130**, 2917–2928.
- Bryan, G. H., J. C. Knievel, and M. D. Parker, 2006: A multimodel assessment of RKW Theory’s relevance to squall-line characteristics. *Mon. Wea. Rev.*, **134**, 2772–2792.
- Bryan, G. H., and R. Rotunno, 2008: The influence of near-surface, high-entropy air in hurricane eyes on maximum hurricane intensity. *J. Atmos. Sci.*, in press.

- Bryan, G. H., J. C. Wyngaard, and J. M. Fritsch, 2003: Resolution requirements for the simulation of deep moist convection. *Mon. Wea. Rev.*, **131**, 2394–2416.
- Davis, C., W. Wang, S. S. Chen, Y. Chen, K. Corbosiero, M. DeMaria, J. Dudhia, G. Holland, J. Klemp, J. Michalakes, H. Reeves, R. Rotunno, C. Snyder, and Q. Xiao, 2008: Prediction of landfalling hurricanes with the Advanced Hurricane WRF Model. *Mon. Wea. Rev.*, **136**, 1990–2005.
- DeMaria, M., and J. Kaplan, 1994: Sea surface temperature and the maximum intensity of Atlantic tropical cyclones. *J. Climate*, **7**, 1324–1334.
- Drennan, W. M., J. A. Zhang, J. R. French, C. McCormick, and P. G. Black, 2007: Turbulent fluxes in the hurricane boundary layer. Part I: Latent heat flux. *J. Atmos. Sci.*, **64**, 1103–1115.
- Emanuel, K. A., 1986: An air–sea interaction theory for tropical cyclones. Part I: Steady-state maintenance. *J. Atmos. Sci.*, **43**, 585–604.
- Emanuel, K. A., 1988: The maximum intensity of hurricanes. *J. Atmos. Sci.*, **45**, 1143–1155.
- Emanuel, K. A., 1989: The finite-amplitude nature of tropical cyclogenesis. *J. Atmos. Sci.*, **46**, 3431–3456.
- Emanuel, K. A., 1994: *Atmospheric Convection*. Oxford, 580 pp.
- Emanuel, K. A., 1995: Sensitivity of tropical cyclones to surface exchange coefficients and a revised steady-state model incorporating eye dynamics. *J. Atmos. Sci.*, **52**, 3969–3976.
- Emanuel, K. A., 1997: Some aspects of hurricane inner-core dynamics and energetics. *J. Atmos. Sci.*, **54**, 1014–1026.
- French, J. R., W. M. Drennan, J. A. Zhang, and P. G. Black, 2007: Turbulent fluxes in the hurricane boundary layer. Part I: Momentum flux. *J. Atmos. Sci.*, **64**, 1089–1102.

- Hausman, S. A., K. V. Ooyama, and W. H. Schubert, 2006: Potential vorticity structure of simulated hurricanes. *J. Atmos. Sci.*, **63**, 87–108.
- Hill, K. A., and G. M. Lackmann, 2008: Analysis of idealized tropical cyclone simulations using the Weather Research and Forecasting Model: Sensitivity to turbulence parameterization and grid spacing. *Mon. Wea. Rev.*, in press.
- Holland, G. J., 1997: The maximum potential intensity of tropical cyclones. *J. Atmos. Sci.*, **54**, 2519–2541.
- Kepert, J. D., 2006a: Observed boundary layer wind structure and balance in the hurricane core. Part I: Hurricane Georges. *J. Atmos. Sci.*, **63**, 2169–2193.
- Kepert, J. D., 2006b: Observed boundary layer wind structure and balance in the hurricane core. Part II: Hurricane Mitch. *J. Atmos. Sci.*, **63**, 2194–2211.
- Klemp, J. B., and R. B. Wilhelmson, 1978: The simulation of three-dimensional convective storm dynamics. *J. Atmos. Sci.*, **35**, 1070–1096.
- Lackmann, G. M., and R. M. Yablonsky, 2004: The importance of the precipitation mass sink in tropical cyclones and other heavily precipitating systems. *J. Atmos. Sci.*, **61**, 1674–1692.
- LeeJoice, R. N., 2000: Hurricane inner-core structure as revealed by GPS dropwindsondes. M.S. thesis, Department of Atmospheric Science, Colorado State University, 56 pp.
- Lin, Y.-L., R. D. Farley, and H. D. Orville, 1983: Bulk parameterization of the snow field in a cloud model. *J. Climate Appl. Meteor.*, **22**, 1065–1092.
- Montgomery, M. T., M. M. Bell, S. D. Aberson, and M. L. Black, 2006: Hurricane Isabel (2003): New insights into the physics of intense storms. Part I: Mean vortex structure and maximum intensity estimates. *Bull. Amer. Meteor. Soc.*, **87**, 1335–1347.

- Morrison, H., G. Thompson, and V. Tatarskii, 2008: Impact of cloud microphysics on the development of trailing stratiform precipitation in a simulated squall line: Comparison of one- and two-moment schemes. *Mon. Wea. Rev.*, in press.
- Ooyama, K. V., 2001: A dynamic and thermodynamic foundation for modeling the moist atmosphere with parameterized microphysics. *J. Atmos. Sci.*, **58**, 2073–2102.
- Persing, J., and M. T. Montgomery, 2003: Hurricane superintensity. *J. Atmos. Sci.*, **60**, 2349–2371.
- Persing, J., and M. T. Montgomery, 2005: Is environmental CAPE important in the determination of maximum possible hurricane intensity? *J. Atmos. Sci.*, **62**, 542–550.
- Powell, M. D., P. J. Vickery, and T. A. Reinhold, 2003: Reduced drag coefficient for high wind speeds in tropical cyclones. *Nature*, **422**, 279–283.
- Qiu, C.-J., J.-W. Bao, and Q. Xu, 1993: Is the mass sink due to precipitation negligible? *Mon. Wea. Rev.*, **121**, 853–857.
- Rosenthal, S. L., 1971: The response of a tropical cyclone model to variations in boundary layer parameters, initial conditions, lateral boundary conditions, and domain size. *Mon. Wea. Rev.*, **99**, 767–777.
- Rotunno, R., Y. Chen, W. Wang, C. Davis, J. Dudhia, and G. J. Holland, 2008: Resolved turbulence in a three-dimensional model of an idealized tropical cyclone. *Geophys. Res. Lett.*, submitted.
- Rotunno, R., and K. A. Emanuel, 1987: An air-sea interaction theory for tropical cyclones. Part II: Evolutionary study using a nonhydrostatic axisymmetric numerical model. *J. Atmos. Sci.*, **44**, 542–561.
- Satoh, M., 2003: Conservative scheme for a compressible nonhydrostatic model with moist processes. *Mon. Wea. Rev.*, **131**, 1033–1050.

- Skamarock, W. C., and J. B. Klemp, 1992: The stability of time-split numerical methods for the hydrostatic and the nonhydrostatic elastic equations. *Mon. Wea. Rev.*, **120**, 2109–2127.
- Walko, R. L., W. R. Cotton, G. Feingold, and B. Stevens, 2000: Efficient computation of vapor and heat diffusion between hydrometeors in a numerical model. *Atmos. Res.*, **53**, 171–183.
- Wang, Y., 2002a: An explicit simulation of tropical cyclones with a triply nested movable mesh primitive equation model: TCM3. Part II: Model refinements and sensitivity to cloud microphysics parameterization. *Mon. Wea. Rev.*, **130**, 3022–3036.
- Wang, Y., 2002b: Vortex Rossby waves in a numerically simulated tropical cyclone. Part II: The role in tropical cyclone structure and intensity changes. *J. Atmos. Sci.*, **59**, 1239–1262.
- Whitney, L. D., and J. S. Hobgood, 1997: The relationship between sea surface temperatures and maximum intensities of tropical cyclones in the Eastern North Pacific. *J. Climate*, **10**, 2921–2930.
- Wicker, L. J., and W. C. Skamarock, 2002: Time splitting methods for elastic models using forward time schemes. *Mon. Wea. Rev.*, **130**, 2088–2097.
- Wu, L., and S. A. Braun, 2004: Effects of environmentally induced asymmetries on hurricane intensity: A numerical study. *J. Atmos. Sci.*, **61**, 3065–3081.
- Yang, B., Y. Wang, and B. Wang, 2007: The effect of internally generated inner-core asymmetries on tropical cyclone potential intensity. *J. Atmos. Sci.*, **64**, 1165–1188.
- Yau, M. K., Y. Liu, D.-L. Zhang, and Y. Chen, 2004: A multiscale numerical study of Hurricane Andrew (1992). Part VI: Small-scale inner-core structures and wind streaks. *Mon. Wea. Rev.*, **132**, 1410–1433.

Zeng, Z., Y. Wang, and C.-C. Wu, 2007: Environmental dynamical control of tropical cyclone intensity – An observational study. *Mon. Wea. Rev.*, **135**, 38–59.

Zhang, D.-L., and E. Altshuler, 1999: The effects of dissipative heating on hurricane intensity. *Mon. Wea. Rev.*, **127**, 3032–3038.

List of Figures

1	The thermodynamic sounding used for this study. Dots are the data used in the simulations by RE87, and lines illustrate interpolation (between points) and extrapolation (downward from the lowest model level) to initialize higher-resolution simulations.	43
2	Maximum azimuthal velocity (v_{\max} , m s^{-1}) from simulations that use different values for l_h and l_v . Shaded boxes denotes settings used by RE87 and PM03.	44
3	Maximum azimuthal velocity (v_{\max} , solid) and maximum gradient wind ($v_{g,\max}$, dashed) from simulations that use different values for l_h (using $l_v = 200$ m). .	45
4	Properties at the top of the boundary layer ($z = 1.1$ km) from simulations that use different values for l_h , as indicated by the legend (using $l_v = 200$ m): (a) angular momentum (M), and (b) equivalent potential temperature (θ_e). Dots indicate the location of v_{\max} in these simulations.	46
5	Output from simulations that use different specification of the turbulence length scales: (a) $l_h = 3000$ m and $l_v = 200$ m; (b) $l_h = 750$ m and $l_v = 200$ m; (c) $l_h = 750$ m and $l_v = 50$ m. Azimuthal velocity is shaded, and radial velocity is contoured every 10 m s^{-1} with negative contours dashed and the zero contour excluded. The minimum value of u is listed at the top of each panel.	47
6	Maximum azimuthal velocity (v_{\max} , m s^{-1}) from simulations that use different ratios of surface exchange coefficients for entropy and momentum, C_E/C_D , using $l_h = 375$ m (solid), $l_h = 1500$ m (dashed), and $l_h = 3000$ m (dotted). The gray line denotes 70 m s^{-1} , which is the approximate maximum intensity observed for this sea surface temperature.	48
7	Maximum azimuthal velocity (v_{\max} , m s^{-1}) from simulations that use different values for terminal fall velocity (V_t , m s^{-1}) using $l_h = 375$ m (solid) and $l_h = 1500$ m (dashed).	49

8	Analyses of the trajectory that passes through v_{\max} plotted over s and q_l from three simulations that use different fall velocities: (a)–(b) are from $V_t = 0 \text{ m s}^{-1}$, (c)–(d) are from $V_t = 7 \text{ m s}^{-1}$, and (e)–(f) are from $V_t = 20 \text{ m s}^{-1}$. The trajectory is illustrated by the thick line, and the dot denotes the location of v_{\max} . Entropy is contoured: s_r is on the left (with contour interval of $40 \text{ J kg}^{-1} \text{ K}^{-1}$), s_p is on the right (with contour interval of $10 \text{ J kg}^{-1} \text{ K}^{-1}$). Shading denotes q_l in g kg^{-1}	50
9	Thermodynamic soundings used for sensitivity analysis: a reversible sounding (solid) and a pseudoadiabatic sounding (dashed). Both soundings are saturated, and both have the same equivalent potential temperature at the surface as the control sounding.	51
10	As in Fig. 7 except the solid line shows results using the conservative equation set and the dashed line shows results using the traditional equation set. The upper set of curves use $l_h = 375 \text{ m}$ and the lower set of curves use $l_h = 1500 \text{ m}$	52
A1	Time series of maximum azimuthal velocity (v_{\max} , m s^{-1}) from two models at two different resolutions, as indicated by legend. To provide a smoother analysis, data are averaged over 3 h.	53

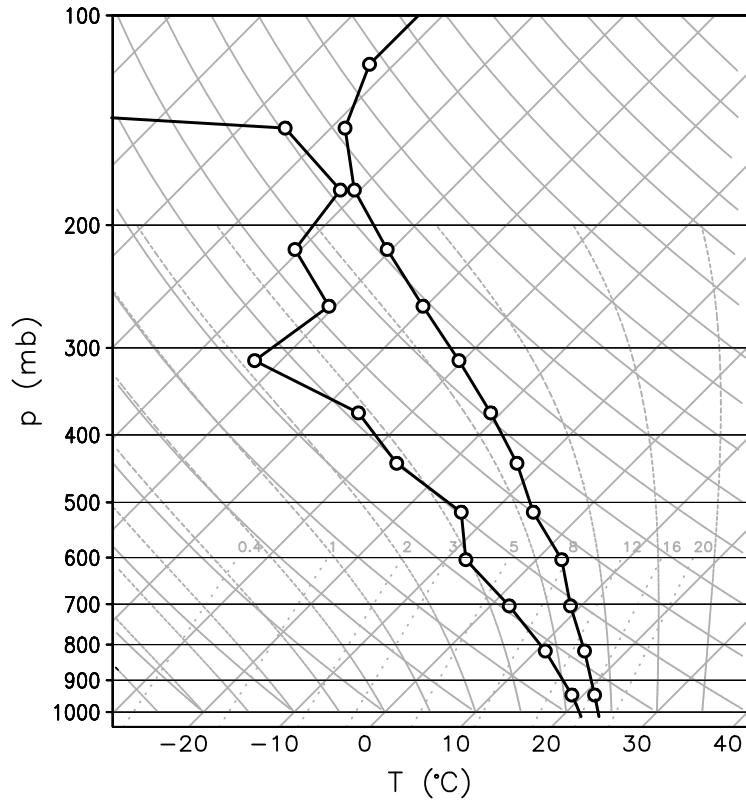


FIG. 1: The thermodynamic sounding used for this study. Dots are the data used in the simulations by RE87, and lines illustrate interpolation (between points) and extrapolation (downward from the lowest model level) to initialize higher-resolution simulations.

		V_{\max} (m s ⁻¹)						
l_v (m)	400	107	105	97	87	72	57	30
	200	108	105	98	86 (PM03)	72	48 (RE87)	33
	100	108	105	98	86	72	47	34
	50	106	101	97	85	73	52	35
	25	108	101	91	82	70	54	41
			94	188	375	750	1500	3000
		l_h (m)						

FIG. 2: Maximum azimuthal velocity (v_{\max} , m s⁻¹) from simulations that use different values for l_h and l_v . Shaded boxes denotes settings used by RE87 and PM03.

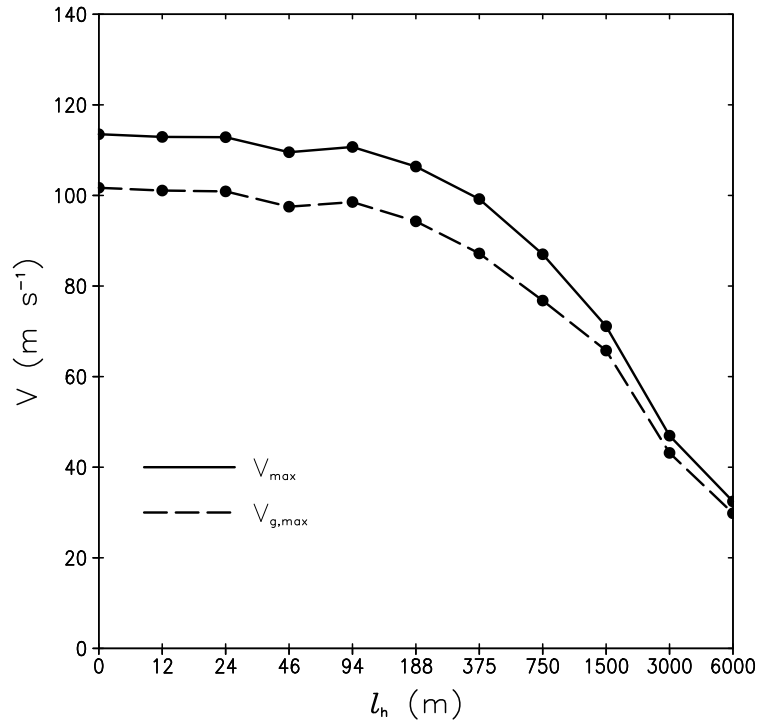


FIG. 3: Maximum azimuthal velocity (v_{\max} , solid) and maximum gradient wind ($v_{g,\max}$, dashed) from simulations that use different values for l_h (using $l_v = 200$ m).

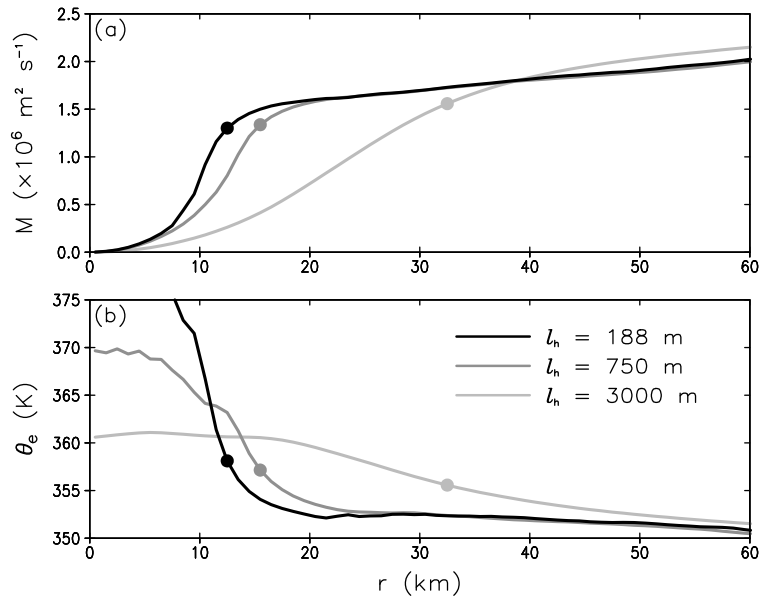


FIG. 4: Properties at the top of the boundary layer ($z = 1.1$ km) from simulations that use different values for l_h , as indicated by the legend (using $l_v = 200$ m): (a) angular momentum (M), and (b) equivalent potential temperature (θ_e). Dots indicate the location of v_{\max} in these simulations.

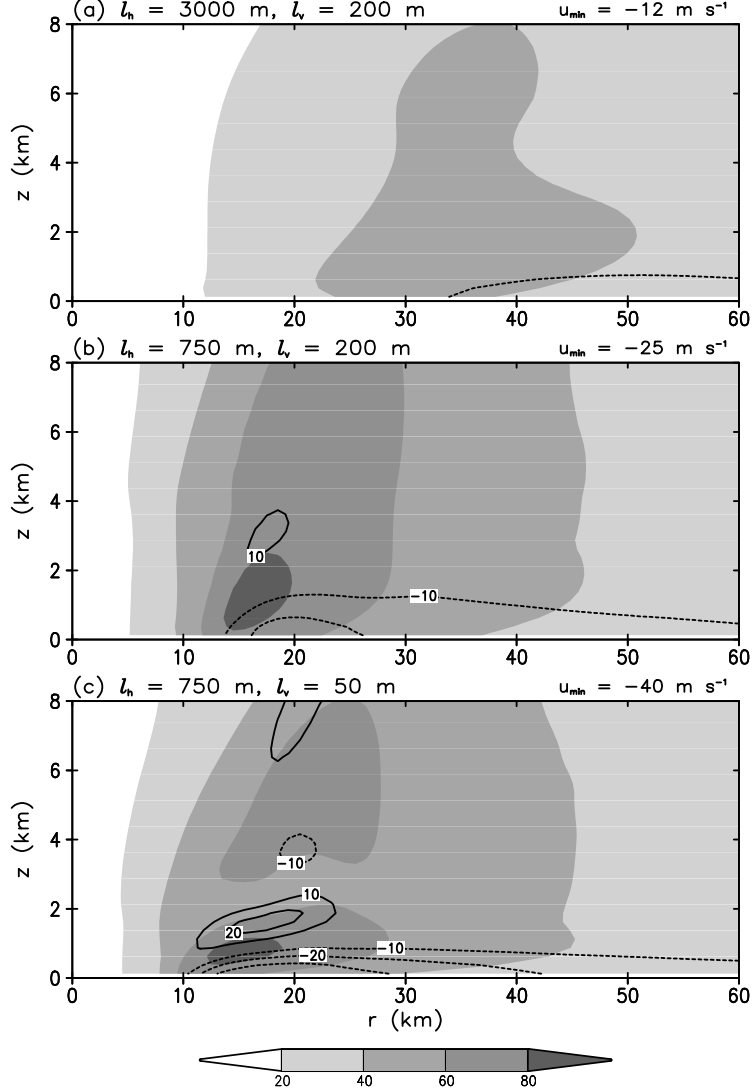


FIG. 5: Output from simulations that use different specification of the turbulence length scales: (a) $l_h = 3000$ m and $l_v = 200$ m; (b) $l_h = 750$ m and $l_v = 200$ m; (c) $l_h = 750$ m and $l_v = 50$ m. Azimuthal velocity is shaded, and radial velocity is contoured every 10 m s $^{-1}$ with negative contours dashed and the zero contour excluded. The minimum value of u is listed at the top of each panel.

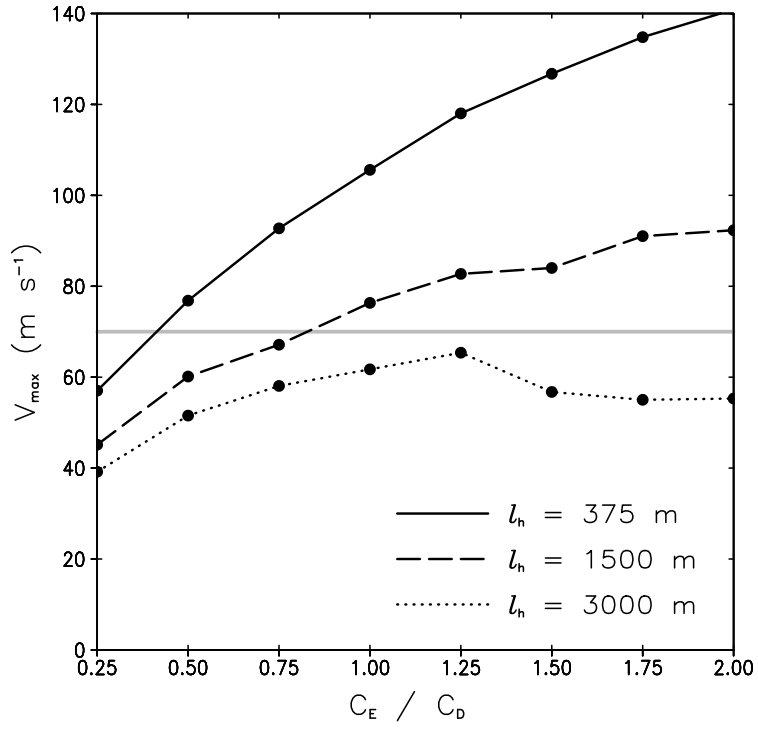


FIG. 6: Maximum azimuthal velocity (v_{\max} , m s⁻¹) from simulations that use different ratios of surface exchange coefficients for entropy and momentum, C_E/C_D , using $l_h = 375$ m (solid), $l_h = 1500$ m (dashed), and $l_h = 3000$ m (dotted). The gray line denotes 70 m s⁻¹, which is the approximate maximum intensity observed for this sea surface temperature.

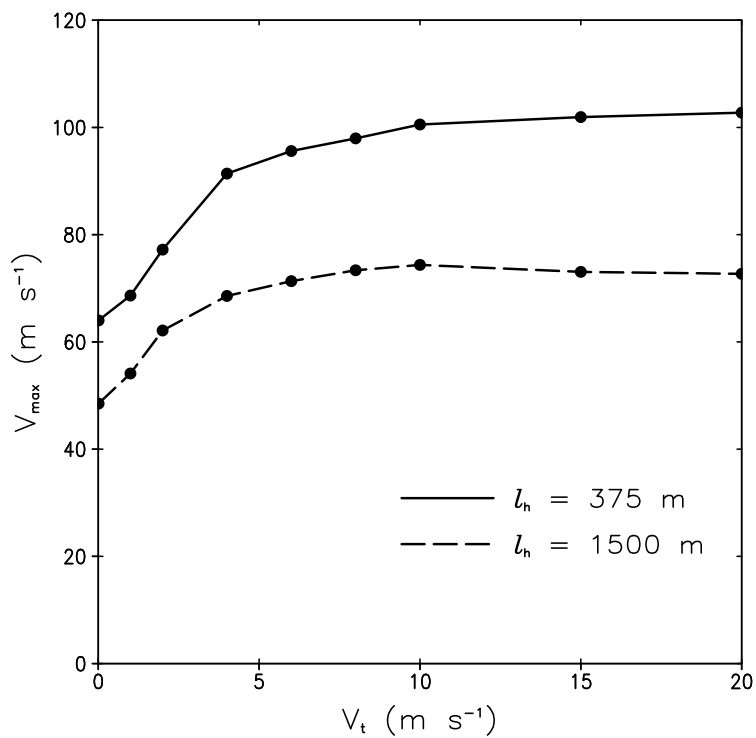


FIG. 7: Maximum azimuthal velocity (v_{\max} , m s⁻¹) from simulations that use different values for terminal fall velocity (V_t , m s⁻¹) using $l_h = 375$ m (solid) and $l_h = 1500$ m (dashed).

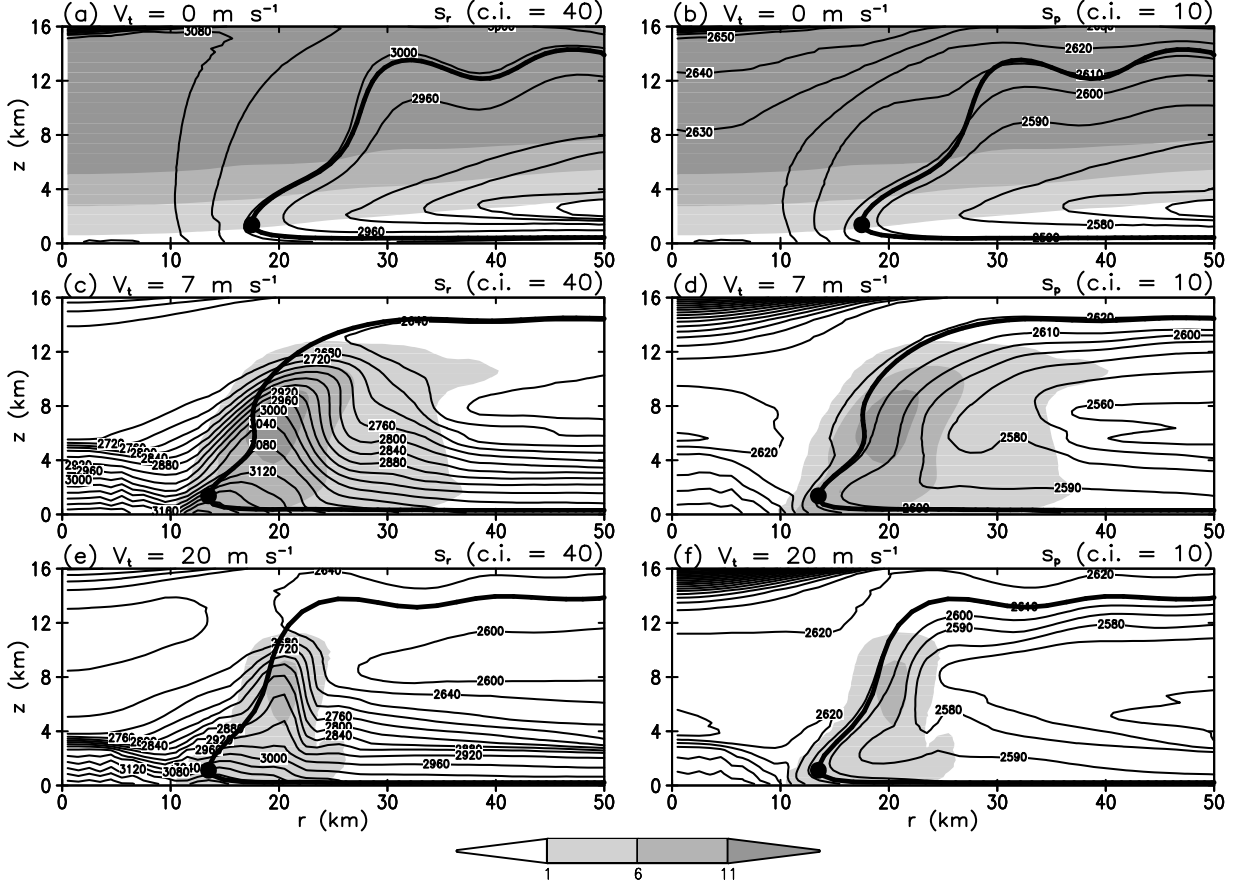


FIG. 8: Analyses of the trajectory that passes through v_{\max} plotted over s and q_l from three simulations that use different fall velocities: (a)–(b) are from $V_t = 0 \text{ m s}^{-1}$, (c)–(d) are from $V_t = 7 \text{ m s}^{-1}$, and (e)–(f) are from $V_t = 20 \text{ m s}^{-1}$. The trajectory is illustrated by the thick line, and the dot denotes the location of v_{\max} . Entropy is contoured: s_r is on the left (with contour interval of $40 \text{ J kg}^{-1} \text{ K}^{-1}$), s_p is on the right (with contour interval of $10 \text{ J kg}^{-1} \text{ K}^{-1}$). Shading denotes q_l in g kg^{-1} .

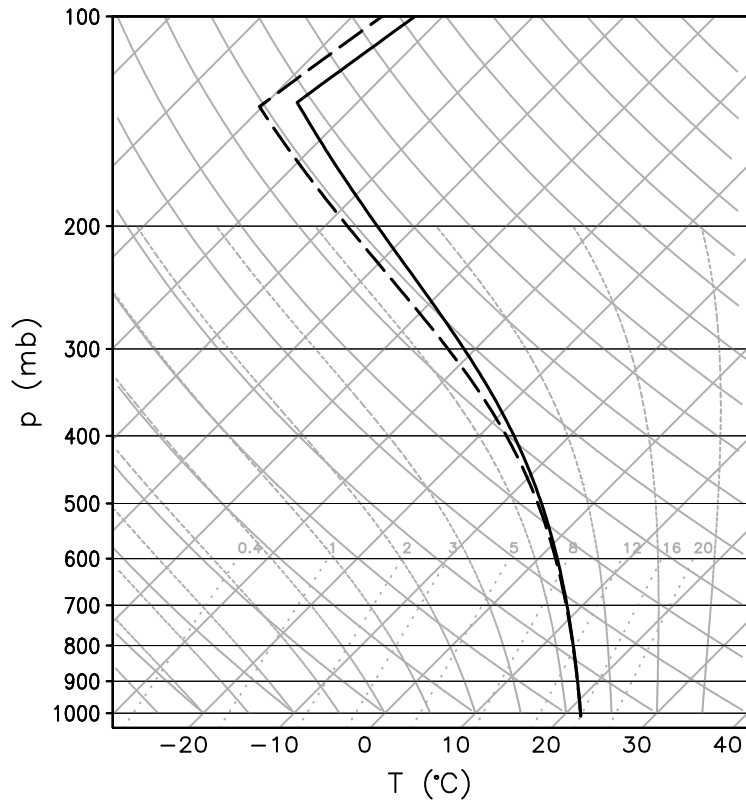


FIG. 9: Thermodynamic soundings used for sensitivity analysis: a reversible sounding (solid) and a pseudoadiabatic sounding (dashed). Both soundings are saturated, and both have the same equivalent potential temperature at the surface as the control sounding.

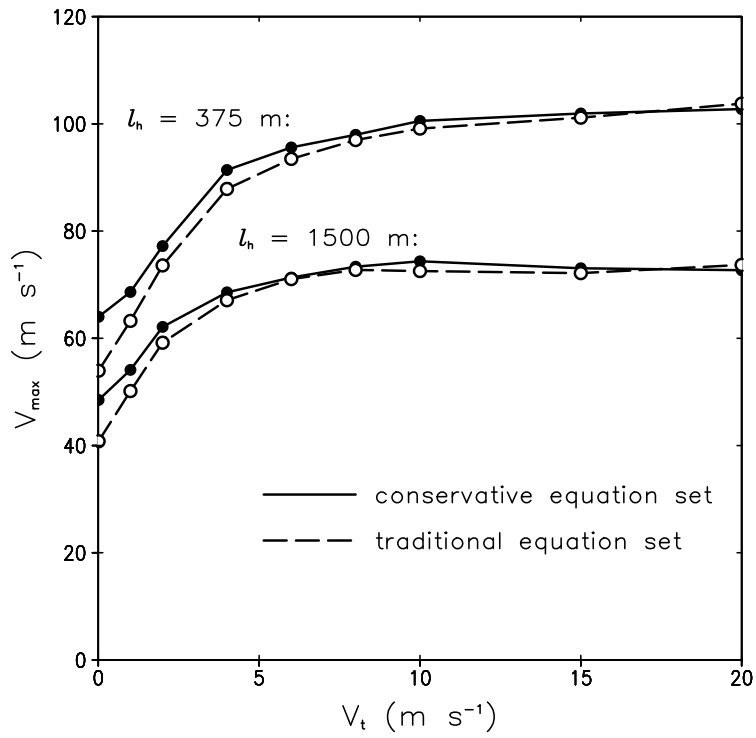


FIG. 10: As in Fig. 7 except the solid line shows results using the conservative equation set and the dashed line shows results using the traditional equation set. The upper set of curves use $l_h = 375$ m and the lower set of curves use $l_h = 1500$ m.

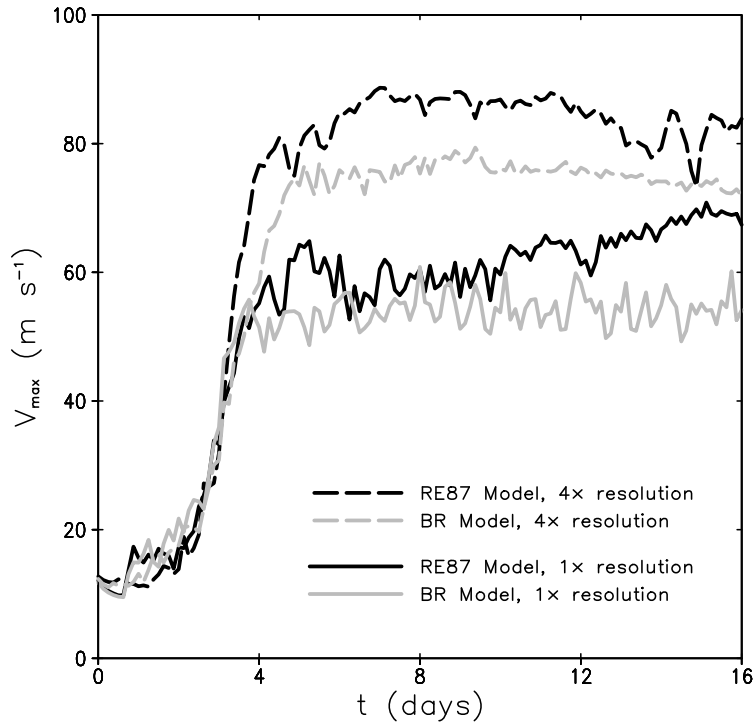


FIG. A1: Time series of maximum azimuthal velocity (v_{\max} , m s^{-1}) from two models at two different resolutions, as indicated by legend. To provide a smoother analysis, data are averaged over 3 h.

Table 1: Summary of model parameters for different configurations, wherein Δr is the radial grid spacing, Δz is the vertical grid spacing, Δt is the timestep, l_h is the horizontal turbulence length scale, and l_v is the vertical turbulence length scale. Unless specified otherwise, the settings under “Default” are used for all results.

Configuration	Δr (km)	Δz (km)	Δt (s)	l_h (m)	l_v (m)
Default	1.0	0.25	7.5	(see text)	(see text)
1x (RE87)	15.0	1.25	20	3000	200
4x (PM03)	3.75	0.3125	5	750	200

Table 2: Maximum azimuthal velocity (v_{\max}) from resolution sensitivity tests.

Δr (m)	Δz (m)	v_{\max} (m s ⁻¹)
Sensitivity to Δr :		
16000	250	70
8000	250	96
4000	250	98
2000	250	100
1000	250	102
500	250	104
Sensitivity to Δz :		
1000	1000	119
1000	500	111
1000	250	102
1000	125	105
1000	63	103

Table 3: Properties from simulations with different radial grid spacing (Δr) using $l_h = 0$ and $l_v = 200$ m: v_{\max} is the maximum azimuthal velocity, and W is the width of the updraft (defined as $w \geq 0.5$ m s $^{-1}$ at $z = 1$ km).

Δr (m)	v_{\max} (m s $^{-1}$)	W (km)
16000	72	32.0
8000	97	16.0
4000	113	8.0
2000	110	8.0
1000	114	9.0
500	114	8.5
250	114	8.5

Table 4: Maximum azimuthal velocity (v_{\max}) from simulations using different environmental soundings and thermodynamics (for $l_h = 375$ m).

Setup: sounding/thermodynamics	v_{\max} (m s ⁻¹)
control / reversible	64
control / pseudoadiabatic	103
reversible / reversible	40
pseudoadiabatic / pseudoadiabatic	104

Table A1: Maximum azimuthal velocity (v_{\max}) from different model configurations. The 4x setup (see Table 1) is used for all simulations.

Model configuration	Description	v_{\max} (m s ⁻¹)
RE87	Unmodified	86.5
BR	Unmodified	77.8
BR-A	Uses constants from RE87 Model	80.0
BR-B	Uses linearized pressure gradient	79.1
BR-C	Uses second-order advection	79.4
BR-ABC	A + B + C	83.1

Table A2: Default values for constants in the two numerical models.

Symbol	Description (units)	BR value	RE87 value
c_l	Specific heat of liquid water ($\text{J kg}^{-1} \text{K}^{-1}$)	4190.0	0
c_p	Specific heat of dry air at constant pressure ($\text{J kg}^{-1} \text{K}^{-1}$)	1005.7	1005.0
c_{pv}	Specific heat of water vapor at constant pressure ($\text{J kg}^{-1} \text{K}^{-1}$)	1870.0	0
c_v	Specific heat of dry air at constant volume ($\text{J kg}^{-1} \text{K}^{-1}$)	718.66	718.0
c_{vv}	Specific heat of water vapor at constant volume ($\text{J kg}^{-1} \text{K}^{-1}$)	1408.5	0
dL_v/dT	Temperature dependence of L_v ($\text{J kg}^{-1} \text{K}^{-1}$)	$c_{pv} - c_l$	0
$L_v(T_0)$	Latent heat of vaporization at $T = T_0$ (J kg^{-1})	2.501×10^6	2.513×10^6
R	Dry air gas constant ($\text{J kg}^{-1} \text{K}^{-1}$)	287.04	287.0
R_v	Water vapor gas constant ($\text{J kg}^{-1} \text{K}^{-1}$)	461.5	461.4
T_0	Reference temperature (K)	273.15	273.0